Environmental Science & Technology

pubs.acs.org/est

Article

Influence of Carbonate Speciation on Hydrated Electron Treatment Processes

Camille K. Amador, Haden Cavalli, Raul Tenorio, Hanna Tetu, Christopher P. Higgins, Shubham Vyas,* and Timothy J. Strathmann*

Cite This: *Environ. Sci. Technol.* 2023, 57, 7849−7857

Read Online

ACCESS | Metrics & More | Article Recommendations | Supporting Information

ABSTRACT: Advanced reduction processes (ARPs) that generate hydrated electrons (e^-_{aq}; e.g., UV-sulfite) have emerged as a promising remediation technology for recalcitrant water contaminants, including per- and polyfluoroalkyl substances (PFASs). The effectiveness of ARPs in different natural water matrices is determined, in large part, by the presence of non-target water constituents that act to quench e^-_{aq} or shield incoming UV photons from the applied photosensitizer. This study examined the pH-dependent quenching of e^-_{aq} by ubiquitous dissolved carbonate species (H_2CO_3*, HCO_3^-, and CO_3^{2-}) and quantified the relative importance of carbonate species to other abundant quenching agents (e.g., H_2O, H^+, HSO_3^-, and $O_{2(aq)}$) during ARP applications. Analysis of laser flash photolysis kinetic data in relation to pH-dependent carbonate acid−base speciation yields species-specific bimolecular rate constants for e^-_{aq} quenching by H_2CO_3*, HCO_3^-, and CO_3^{2-} ($k_{H_2CO_3^*} = 2.23 \pm 0.42 \times 10^9$ M^{-1} s^{-1}, $k_{HCO_3^-} = 2.18 \pm 0.73 \times 10^6$ M^{-1} s^{-1}, and $k_{CO_3^{2-}} = 1.05 \pm 0.61 \times 10^5$ M^{-1} s^{-1}), with quenching dominated by H_2CO_3* (which includes both $CO_{2(aq)}$ and H_2CO_3) at moderately alkaline pH conditions despite it being the minor species. Attempts to apply previously reported rate constants for e^-_{aq} quenching by $CO_{2(aq)}$, measured in acidic solutions equilibrated with $CO_{2(g)}$, overpredict quenching observed in this study at higher pH conditions typical of ARP applications. Moreover, kinetic simulations reveal that pH-dependent trends reported for UV-sulfite ARPs that have often been attributed to e^-_{aq} quenching by varying $[H^+]$ can instead be ascribed to variable acid−base speciation of dissolved carbonate and the sulfite sensitizer.

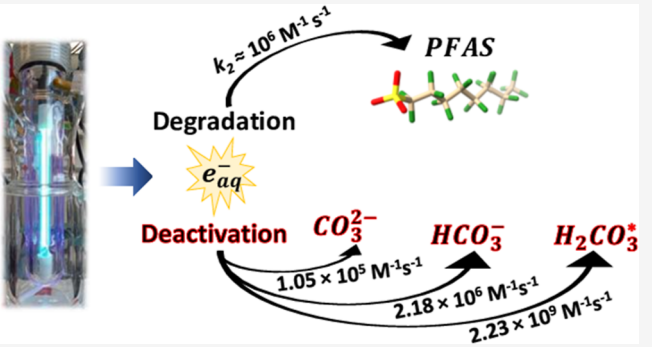

KEYWORDS: *laser flash photolysis, hydrated electron, advanced reduction process, PFAS, acid−base speciation*

INTRODUCTION

Advanced reduction processes (ARPs) are a class of water treatment technologies that integrate activation methods (e.g., UV light and ultrasound) with reduced species (e.g., sulfite and dithionite) to generate reductive radicals that are highly reactive with many aquatic contaminants.[1] Remediation strategies employing ARPs are emerging as promising options for chemicals that are resistant to oxidation, including per- and polyfluoroalkyl substances (PFASs), chlorinated solvents (e.g., trichloroethylene), and toxic oxyanions (e.g., ClO_4^-, BrO_3^-, and CrO_4^{2-}).[2−8] Among ARPs, UV photochemical processes that generate hydrated electrons (e^-_{aq}) have received growing attention due to their potential for degrading highly recalcitrant PFASs.[9] Absorption of UV photons of sufficient energy by an appropriate photosensitizer species (e.g., sulfite, iodide, and ferrocyanide) leads to electron ejection into the bulk solvent, forming e^-_{aq}, a powerful reductant ($E_H^0 = -2.9$ V).[10,11] Practical remediation applications have focused on UV activation with sulfite (SO_3^{2-}) salts due to their low cost as well as the non-toxicity and ubiquity of the byproduct sulfate in natural water systems. Moreover, sulfite has the added benefit of scavenging dissolved oxygen,[12] a known quencher of e^-_{aq} ($k_2 = 1.9 \times 10^{10}$ M^{-1} s^{-1}),[13] and has an extensive history of use at wastewater treatment facilities for dechlorination of treated wastewater before discharging.[14]

While e^-_{aq} is a strong reductant that is able to react with many contaminants of concern, it is also a transient species (lifetime ~10^{-6} s)[15,16] that is rapidly quenched by water and other non-target constituents commonly measured in groundwater, including $O_{2(aq)}$, H^+, and NO_3^-.[17−19] The effectiveness of UV-sulfite and other ARPs in treating target contaminants is directly related to e^-_{aq} steady-state concentrations, which are

Received: December 14, 2022
Revised: May 1, 2023
Accepted: May 2, 2023
Published: May 12, 2023

highly dependent on source water composition and difficult to predict a priori from available information. Moreover, the literature does not currently have the tools to estimate e_{aq}^- steady-state concentrations from geochemical solution conditions. Applications involving e_{aq}^- for contaminant remediation typically require adjustment of pH to alkaline conditions (e.g., pH ≥ 9),[20] often assumed to be a requirement to limit e_{aq}^- quenching by H^+ (2.3×10^{10} M^{-1} s^{-1}).[13,21,22] In fact, Bentel and co-workers recently reported that UV-sulfite treatment of PFASs is dramatically accelerated by increasing pH to 12.[23] Whereas ~85% defluorination of trifluoroacetate was observed after 24 h of reaction at pH 9.5, complete defluorination was observed within 4 h at pH 12.[23] Although pH-dependent trends have often been attributed solely to changes in e_{aq}^- quenching by H^+,[20,22,23] quantitative analysis of reactivity trends does not support this conclusion. For example, our recent work using laser flash photolysis (LFP) demonstrated invariance of e_{aq}^- lifetime from 9 < pH < 12, suggesting that H^+ itself is not a significant e_{aq}^- quencher at these pH conditions.[24] Additional work has highlighted the potential importance of weak acids as alternative quenchers of e_{aq}^- in both laboratory-prepared solutions and real-world water matrices.[25,26] Weak acids exhibit pH-dependent changes in speciation that could influence rates of contaminant degradation observed in different solution matrices. For example, Maza and co-workers recently showed that HSO_3^-, the conjugate acid species of the sulfite photosensitizer (pK_a 7.2),[12,27] is a significant quencher of e_{aq}^- (1.2×10^8 M^{-1} s^{-1})[25] that will inhibit contaminant reactions to varying degrees during UV-sulfite treatment applications, depending on pH conditions.

Perhaps the most ubiquitous weak acids in natural water systems are carbonate species that are in equilibrium with atmospheric $CO_{2(g)}$ (e.g., H_2CO_3* and HCO_3^-) and are a dominant pH buffer of natural water systems. Moreover, carbonate has been widely used in laboratory ARP studies to buffer pH conditions,[23,28−30] and the results of a recent study show that increasing carbonate concentrations inhibit defluorination of perfluorooctanoic acid (PFOA) by e_{aq}^-.[31] While past reports of e_{aq}^- quenching by HCO_3^- ($<10^6$ M^{-1} s^{-1})[32] and CO_3^{2-} (3.9×10^5 M^{-1} s^{-1})[33] suggest such species are unlikely to inhibit contaminant reactions with e_{aq}^- when present at environmentally relevant concentrations, dissolved CO_2 has been reported to react with e_{aq}^- at near diffusion-limited rates (7.7×10^9 M^{-1} s^{-1}).[34] However, it remains unclear whether $CO_{2(aq)}$ (the major contributor to H_2CO_3*), a minor contributor to dissolved carbonate speciation at pH conditions typical of ARP applications, contributes significantly to scavenging in e_{aq}^- treatment processes. Past reports of e_{aq}^- reactions with carbonate assumed quenching by single species, ignoring potential for simultaneous reactions with different (and otherwise minor) acid−base carbonate species that are in equilibrium with the species that predominates at a given pH condition. Thus, given the ubiquity of dissolved carbonate in natural water matrices, a more comprehensive study of e_{aq}^- quenching over a range of pH conditions typical of ARP applications that carefully quantify the effects of changing acid−base-driven carbonate speciation is warranted. Accurate rate constants for e_{aq}^- reactions with individual carbonate species will be critical inputs for comprehensive kinetic models for ARP remediation applications that require a full accounting of sources and sinks of e_{aq}^- in different water matrices.

In this study, we report on the effects of dissolved carbonate concentration and speciation on e_{aq}^- reactions. The inhibitory effect of dissolved carbonate on UV-sulfite treatment of perfluorooctane sulfonate (PFOS), a highly recalcitrant PFAS, was first confirmed and compared with recent reports for PFOA. LFP experiments were then conducted to quantify e_{aq}^- quenching by dissolved carbonate over a range of pH conditions (pH 5−12), and the resulting data were quantitatively analyzed in terms of changing acid−base carbonate speciation. Finally, species-specific bimolecular rate constants derived from this effort were then applied to quantify the potential contribution of dissolved carbonate species relative to other documented quencher species present during treatment applications, including H^+ and HSO_3^-.

MATERIALS AND METHODS

Chemicals. A full list of chemicals used are provided in the Supporting Information. All stock solutions were prepared inside an anaerobic chamber (Coy Lab Products; 97% N_2, 3% H_2) using deoxygenated deionized water prepared as described in the Supporting Information.

Constant Irradiation Experiments. UV-sulfite reaction of PFOS was carried out in solutions amended with varying concentrations of dissolved carbonate. Experiments were conducted using a light source and reactor described previously.[28] Briefly, a jacketed glass photoreactor and jacketed quartz immersion well were used with an 18 W low-pressure Hg UV lamp. Photochemical parameters (photon flux, path length, etc.) were reported previously.[28] A solution containing 70 μg/L PFOS and sulfite (3 mM Na_2SO_3) was buffered at pH 10.0 (5 mM sodium tetraborate) and amended with 0−25 mM $NaHCO_3$ with an NaCl offset to keep the ionic strength constant (0.05 M) across experiments. To eliminate e_{aq}^- scavenging by dissolved oxygen, solutions were deoxygenated by sparging with $N_{2(g)}$ for 1 h before introducing PFOS and sulfite to initiate UV reactions. Sample aliquots were collected at pre-determined time intervals to measure changing PFOS concentrations which were measured by liquid chromatography with tandem mass spectrometry (LC−MS/MS) using procedures and instrumentation described elsewhere.[35] Solution pH was re-measured after the reaction was completed to evaluate any pH drift during experiments. Additional details on reaction solution preparation and analysis are described in the Supporting Information. We note that UV-sulfite treatment often requires millimolar concentrations of Na_2SO_3 as a UV sensitizer, which results in high ppm levels of residual sulfate byproducts that could increase total dissolved solid levels in any receiving water. This, among other reasons, is why it has been suggested to apply destructive technologies, including UV-sulfite,[36] to PFAS concentrate streams (e.g., membrane rejection) rather than for direct treatment of more dilute water sources. Subsequent discharge of small volumes of treated concentrates would then benefit from significant dilution effects.

LFP Experiments. Transient absorption spectra at 690 nm were collected (LP980 spectrophotometer equipped with an ICCD camera and photomultiplier tube, Edinburgh Instruments) to quantify the kinetics of e_{aq}^- quenching in solutions amended with varying sodium bicarbonate concentrations (0−500 mM) and adjusted to varying pH conditions (5.0−12.0). A Nd/YAG laser (Surelite EX, Continuum) operating at 1064 nm with a 10 Hz repetition rate was used with a 4th harmonic generator to produce 266 nm light (further details described elsewhere).[24] Generation of e_{aq}^- was achieved by irradiating a solution of $K_4Fe(CN)_6$ (40 μM) and $K_3Fe(CN)_6$ (10 μM)

https://doi.org/10.1021/acs.est.2c09451
Environ. Sci. Technol. 2023, 57, 7849−7857

with an 8−10 mJ laser pulse. Ten transient spectra were measured and averaged for each of the solution. Unless otherwise noted, individual solutions containing $K_4Fe(CN)_6$, $K_3Fe(CN)_6$, the desired bicarbonate concentration, and NaCl (added to fix ionic strength near 0.5 M), were prepared in 50 mL polypropylene centrifuge tubes and adjusted to the desired pH condition using either 1 M HCl or NaOH. Three replicate 2.75 mL aliquots of each solution were then transferred to individual quartz cuvettes (Innovative Lab Supply) and sealed before removing them from the anaerobic chamber and subjecting them to LFP measurement. Stern−Volmer analysis of the change in e^-_{aq} lifetime (τ) for all 15 measurements was used to determine the pH-dependent k_{app} value. Further details on solution preparation can be found in the Supporting Information.

A separate LFP experiment was conducted to measure e^-_{aq} quenching by dissolved H_2CO_3* (which includes both $CO_{2(aq)}$ and H_2CO_3) under acidic pH conditions. A stock solution of 31.8 mM H_2CO_3* was prepared inside the anaerobic chamber by sparging deionized water with 1 atm $CO_{2(g)}$ overnight; H_2CO_3* concentration was estimated using the Henry's Law constant for $CO_{2(g)}$ (3.4×10^{-2} mol/kg bar at 20 °C).[37] Aliquots of varying volume from this stock solution were mixed in a cuvette with solution containing $K_4Fe(CN)_6$, $K_3Fe(CN)_6$, and electrolyte to yield final concentrations equal to the other experiments (i.e., 40 μM $K_4Fe(CN)_6$, 10 μM $K_3Fe(CN)_6$, ionic strength ≈ 0.5 M) and then immediately sealed with minimal headspace (3.5 mL total) before removing from the glovebox for LFP analysis of e^-_{aq} lifetimes. Replicate solutions were prepared in larger centrifuge tubes to measure pH of the solution before the reaction, and the 3.5 mL samples were pooled post reaction to measure the pH after LFP analysis.

Analysis and Modeling. PFOS degradation kinetics observed in constant irradiation experiments followed a pseudo-first-order rate law, and corresponding rate constants (k_{obs}, h^{-1}) were determined by least-squares fits of the model to measurements. Apparent bimolecular rate constants for e^-_{aq} quenching by dissolved carbonate species at each pH condition (k_{app}, M^{-1} s^{-1}) were derived from LFP data using Stern−Volmer analyses of the changes in e^-_{aq} lifetimes (τ) as a function of total dissolved carbonate concentration (C_{T,CO_3}). Equilibrium acid−base speciation of dissolved carbonate and sulfite was calculated using Visual MINTEQ (Ver 3.1). MINTEQ calculations assumed an ionic strength (μ) of 0.5 M for LFP experiments, 0.05 M for the constant irradiation experiments, and a temperature of 20 °C for both. Species-specific carbonate-e^-_{aq} bimolecular rate constants were then determined by least-squares fits of the trends in measured k_{app} values in relation to carbonate speciation (Scientist Ver 3.0, Micromath Research). Scientist was also used to rule out the potential kinetic limitations of carbonate species interconversion reactions to the observed kinetics of e^-_{aq} quenching.

RESULTS AND DISCUSSION

Effect of Dissolved Carbonate on PFAS Degradation. Here, we first re-visited the effects of dissolved carbonate on the kinetics of e^-_{aq} ARP PFAS degradation by examining treatment of PFOS during UV-sulfite treatment, a commonly applied ARP. In the absence of added carbonate, UV-sulfite treatment of PFOS with 3 mM sulfite (pH 10.0) yielded a k_{obs} value of 0.237 ± 0.031 h^{-1}. This value dropped by >25% (0.154 ± 0.035 h^{-1}) and >50% (0.105 ± 0.027 h^{-1}) when 1 and 5 mM total dissolved carbonate, respectively, were added to the solution and pH was kept constant (Figure 1). These

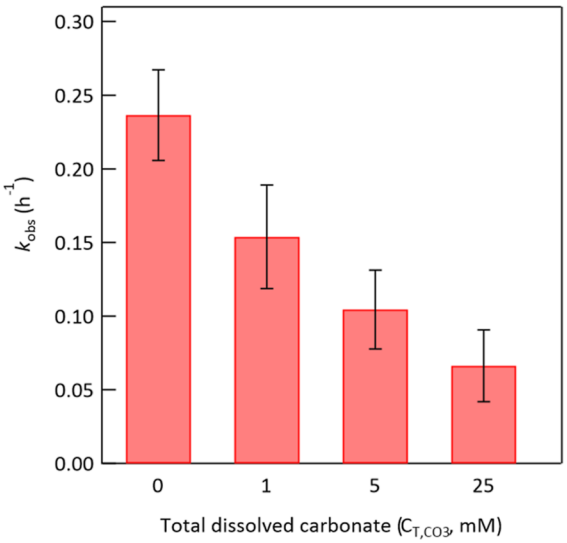

Figure 1. Effect of added dissolved carbonate on the observed rate constant for PFOS degradation during UV-sulfite treatment. Reaction conditions: $[PFOS]_{initial}$ = 70 μg/L, 3 mM Na_2SO_3, irradiation with LP-Hg light source, pH 10.0 (5 mM borate buffer), 20 °C. Each experimental condition was run in duplicate, and error bars represent the standard deviation of k_{obs} values determined from duplicate experiments conducted under the same conditions.

decreases in k_{obs} are particularly noteworthy since mM concentrations have often been applied to buffer pH in previous studies examining UV-sulfite treatment of PFASs.[23,28−30] Moreover, this highlights that environmentally relevant concentrations of dissolved carbonate can inhibit PFAS degradation. Additionally, the pseudo-first-order reaction rate constant (k_{obs}; h^{-1}) obtained here for 5 mM added carbonate is not far off from previous reports by Tenorio and co-workers at similar conditions (0.080 ± 0.005 h^{-1}).[28] Further increases in carbonate concentration led to greater inhibition, where k_{obs} = 0.066 ± 0.024 h^{-1} when 25 mM carbonate was added. It should be noted that removal of dissolved carbonate resulting from dissolution of ambient $CO_{2(g)}$ was not attempted because it would be difficult to ensure complete removal experimentally. However, the concentration of dissolved carbonate expected to be present in equilibrium with atmospheric $CO_{2(g)}$ (~10^{-5} M) is far lower than the concentrations of carbonate added in these experiments (1−25 mM). Moreover, any background levels of dissolved carbonate will be the same for each condition shown in Figure 1, so differences between the k_{obs} at the various C_{T,CO_3} are still valid.

These findings are also consistent with earlier reports noting inhibited rates of PFAS treatment by e^-_{aq} ARPs. Ren et al. investigated the effect of carbonate, as well as other common, co-existing anions, on degradation and defluorination of PFOA, a commonly studied long-chain perfluoroalkyl carboxylic acid.[31] In the absence of carbonate, nearly 100% degradation of PFOA was observed within 1 h, while only about 55% of PFOA was degraded during the same time in the presence of 5 mM added carbonate, the lowest concentration studied. Not only was carbonate found to inhibit parent compound degradation, but it also decreased the extent of

https://doi.org/10.1021/acs.est.2c09451
Environ. Sci. Technol. 2023, 57, 7849−7857

PFOA defluorination from nearly 90% (0 mM) to ~60% (5 mM) after 24 h. Further increases in carbonate concentration, up to 25 mM, led to further inhibition.

LFP Measurements. The progressive inhibition of PFOS degradation observed with increasing total dissolved carbonate is consistent with competitive scavenging of the reactive e^-_{aq} by this solution component. Given the ubiquity of carbonate species in natural water matrices, this warrants further investigation to better predict its influence on treatment efficacy. LFP kinetic traces collected for e^-_{aq} quenching in solutions buffered at pH 9.3 and varying concentrations of carbonate are provided in Figure 2A (traces for all other pH conditions provided in the Supporting Information). Following excitation, absorbance values at 690 nm (characteristic of e^-_{aq}[38]) increase to an initial optical density (ΔOD) value of ~0.05. Applying Beer's law and reported molar absorptivity for e^-_{aq} at 690 nm (20,560 M^{-1} cm^{-1}),[39,40] each laser pulse generated an initial e^-_{aq} concentration of ~2.4 μM. We note that the amount of e^-_{aq} generated is at least 1000× lower than that of the added quencher which varied from 2.5 to 500 mM C_{T,CO_3} (see Figure S9). Therefore, any reactions between carbonate and adventitious reactive species (e.g., $H^\bullet$) will not affect the kinetics of the reaction of interest since carbonate is in significant excess. Absorbance then decays on a μs timescale and was accelerated by the addition of increasing concentrations of total dissolved carbonate. Rate constants were determined in a similar fashion as our previous study,[24] and results of the replicate measurements were found to be highly reproducible. Briefly, lifetimes of the transient e^-_{aq} species (τ; ns) were analyzed using a Stern–Volmer type relationship (i.e., $1/\tau$ vs C_{T,CO_3}; Figure 2B,C) to derive apparent bimolecular rate constants (k_{app}; M^{-1} s^{-1}) for e^-_{aq} reactions with dissolved carbonate at each pH condition. Table 1 summarizes k_{app} measured at various pH conditions from pH 5.0 to 12.

The results of these experiments show that values of k_{app} increase dramatically with decreasing pH conditions, with values increasing from $<2 \times 10^5$ M^{-1} s^{-1} at pH 12.0 to $4.63 (\pm 0.13) \times 10^9$ M^{-1} s^{-1} for pH 5–5.5 prepared by equilibrating solutions with $CO_{2(g)}$ (Figure 2C). We note that the continued increase in k_{app} at pH < 6 is possibly a consequence of uncertainties in the H_2CO_3* concentrations estimated from Henry's law when performing Stern–Volmer analysis and not to an actual increase in carbonate reactivity or e^-_{aq} quenching by H^+ (vide infra). This trend is attributed to changes in the acid–base speciation of the dissolved carbonate species. The predominance of e^-_{aq} quenching by carbonate species is further supported by the fact that the measured lifetimes for e^-_{aq} (τ; μs) in the absence of added carbonate show little change in value between pH 5.8 and 12.0 (Figure S2), highlighting that H^+, which varies 10-fold in concentration for each integer change in pH, is not a major quencher species compared to the solvent and the photosensitizer species. It follows that dissolved carbonate and its speciation may be determinative factors in the reported pH dependencies of e^-_{aq}-based ARPs,[23,31,41] rather than variable $[H^+]$.

Quantitative Analysis of Kinetics in Terms of Carbonate Speciation. Figure 3 shows the measured values of k_{app} as a function of pH along with fits of a model that assumes parallel reactions of e^-_{aq} with different species of dissolved carbonate. As a diprotic acid, dissolved carbonate speciation can be described by acid dissociation constants

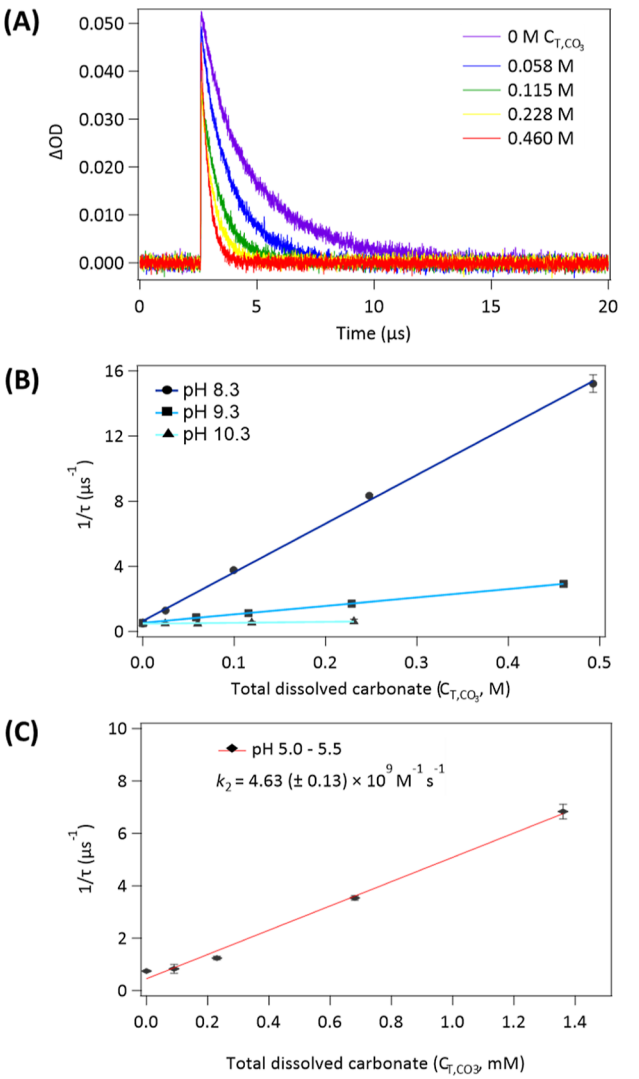

Figure 2. (A) Kinetic transient absorption traces for e^-_{aq} decay (measured at 690 nm) at pH 9.3 in solutions amended with varying concentrations of dissolved carbonate prepared from $NaHCO_3$. Solution conditions: 40 μM $K_4Fe(CN)_6$, 10 μM $K_3Fe(CN)_6$, ionic strength = 0.47 M (balanced using NaCl). (B) Stern–Volmer plots for selected pH conditions generated from model fits of the traces to determine e^-_{aq} lifetimes in each solution (results for all pH conditions provided in the Supporting Information). (C) Stern–Volmer plot for acidic solutions (pH 5.0–5.5) prepared by equilibrating $CO_{2(g)}$ with aqueous solutions and then adding $K_4Fe(CN)_6$, $K_3Fe(CN)_6$, and NaCl. Individual kinetic traces in panel (A) represent the average of the triplicate measurements, and error bars in panels (B) and (C) represent one standard deviation based upon triplicate measurements. Apparent rate constants derived from Stern–Volmer analyses provided in Table 1.

$$H_2CO_3^* \rightleftarrows H^+ + HCO_3^-;\ pK_{a_1} = 6.35 \quad (1)$$

$$HCO_3^- \rightleftarrows H^+ + CO_3^{2-};\ pK_{a_2} = 10.33 \quad (2)$$

Therefore, speciation shifts from predominantly H_2CO_3* (includes both $CO_{2(aq)}$ and H_2CO_3, with the former accounting for >99% of the total) at the lowest pH conditions examined to predominantly HCO_3^- at pH conditions between the two pK_a values and finally to predominantly CO_3^{2-} at the highest pH conditions examined. We note that the pK_a values cited above are for standard conditions (e.g., 25 °C, 1 atm, 0 M

https://doi.org/10.1021/acs.est.2c09451
Environ. Sci. Technol. 2023, 57, 7849–7857

Table 1. Summary of k_{app} Values Determined at Various pH Conditions Using LFP along with Corresponding α Values at Each Condition Determined Using Visual MINTEQ at an Ionic Strength (μ) of 0.5 M and Temperature Fixed at 20 °C

pH	μ (M)	C^{max}_{T,CO_3} (M)	α_0	α_1	α_2	k_{app} ($M^{-1}s^{-1}$)
12.0	0.54	0.33	1.47×10^{-8}	0.009	0.991	$1.54\ (\pm1.13) \times 10^5$
11.0	0.52	0.33	1.36×10^{-6}	0.086	0.914	$1.81\ (\pm1.08) \times 10^5$
10.3	0.50	0.23	2.54×10^{-5}	0.321	0.679	$5.91\ (\pm2.30) \times 10^5$
9.8	0.45	0.44	1.50×10^{-4}	0.599	0.401	$1.37\ (\pm0.11) \times 10^6$
9.5	0.46	0.47	3.73×10^{-4}	0.748	0.251	$3.62\ (\pm0.13) \times 10^6$
9.3	0.47	0.46	6.52×10^{-4}	0.825	0.175	$5.18\ (\pm0.12) \times 10^6$
8.8	0.49	0.49	2.34×10^{-3}	0.935	0.063	$1.34\ (\pm0.04) \times 10^7$
8.3	0.50	0.49	7.69×10^{-3}	0.972	0.021	$2.99\ (\pm0.04) \times 10^7$
7.8	0.50	0.50	0.024	0.969	6.49×10^{-3}	$5.54\ (\pm0.15) \times 10^7$
7.3	0.47	0.45	0.073	0.925	1.96×10^{-3}	$1.02\ (\pm0.03) \times 10^8$
6.8	0.55	0.05	0.200	0.800	5.35×10^{-4}	$2.45\ (\pm0.15) \times 10^8$
6.3	0.56	0.05	0.442	0.558	1.18×10^{-4}	$6.65\ (\pm0.32) \times 10^8$
5.8	0.50	0.01	0.714	0.286	1.91×10^{-5}	$1.13\ (\pm0.09) \times 10^9$
5.0–5.5[a]	0.47	0.0014	0.94–0.83	0.06–0.17	$<6 \times 10^{-6}$	$4.63\ (\pm0.13) \times 10^9$

[a]Solution pH varied from 5.0 to 5.5 as concentration of H_2CO_3* stock solution, prepared by equilibrating water with 1 atm CO_2(g), added to unbuffered solution decreased.

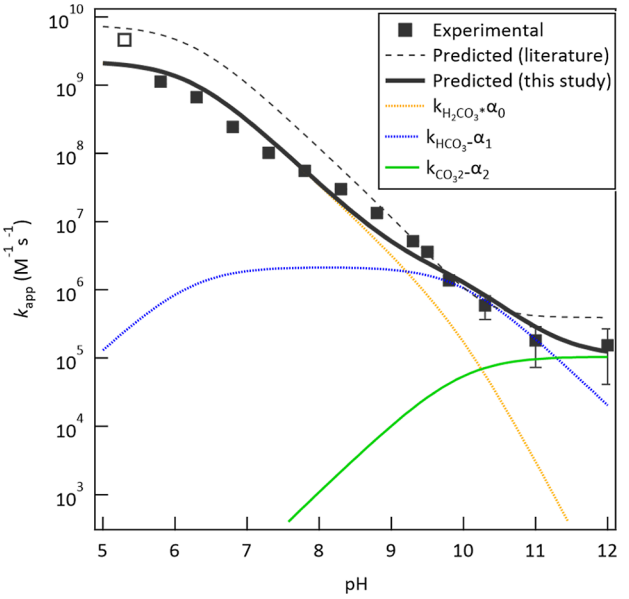

Figure 3. Effect of pH on measured and model-predicted apparent rate constants for e^-_{aq} reaction with dissolved carbonate species. Measured k_{app} for carbonate species at acidic conditions (which ranged from pH 5.0–5.5 with decreasing amounts of added $CO_{2(aq)}$ saturated solution) is shown as an open black square and was prepared by equilibrating water with 1 atm $CO_{2(g)}$. Simulated contributions of H_2CO_3* (beveled orange line), HCO_3^- (beveled blue line), and CO_3^{2-} (beveled green line) to the overall quenching (solid black line) are also shown. The dashed black line shows model predictions using rate constants previously reported in the literature.[33,42,43]

ionic strength); however, the α values reported in Table 1 and throughout these studies were calculated at the conditions applied in the experiments (described in the caption). Figure S3 in the Supporting Information depicts the speciation shifts in our system. It is in line with the observed pH dependence of kinetic trends that e^-_{aq} reactivity follows: H_2CO_3* > HCO_3^- > CO_3^{2-}. If we consider that e^-_{aq} reacts in parallel with individual carbonate species, we can formulate a relationship between k_{app} and the species-specific bimolecular rate constants ($k_{H_2CO_3^*}$, $k_{HCO_3^-}$, and $k_{CO_3^{2-}}$, M^{-1} s^{-1})

$$k_{app} = k_{H_2CO_3^*}\alpha_0 + k_{HCO_3^-}\alpha_1 + k_{CO_3^{2-}}\alpha_2 \quad (3)$$

where the α values represent the fractional contribution of the corresponding species to total dissolved carbonate. Attempts to apply the model described in eq 3 using literature values of $k_{H_2CO_3^*}$ (7.7×10^9 M^{-1} s^{-1}),[42] $k_{HCO_3^-}$ (6×10^5 M^{-1} s^{-1}),[32] and $k_{CO_3^{2-}}$ (3.9×10^5 M^{-1} s^{-1})[33,42,43] reported by separate investigators were unsuccessful. Although the general trend of increasing reactivity with decreasing pH is predicted, the modeled k_{app} values overpredict measurements by up to a factor ~2 over the entire pH range examined (Figure 3, dashed line). The overprediction may result from the fact that past studies measuring carbonate reactivity with e^-_{aq} only considered contributions from a single species in each study. Most importantly, model predictions are dominated by extrapolation of the reported $k_{H_2CO_3^*}$ value measured under acidic pH conditions to much higher pH conditions that are representative of conditions used for ARPs in practice (e.g., pH > 9). This extrapolation leads to overprediction of e^-_{aq} quenching even if it is assumed to be the only species present across the pH range studied (Figure S4).

Re-fitting of eq 3 to the measured k_{app} values in this study yields updated values for $k_{H_2CO_3^*}$ = 2.23 (±0.42) × 10^9 M^{-1} s^{-1}, $k_{HCO_3^-}$ = 2.18 (±0.73) × 10^6 M^{-1} s^{-1}, and $k_{CO_3^{2-}}$ = 1.05 (±0.61) × 10^5 M^{-1} s^{-1} that more closely match the observed e^-_{aq} quenching over the full range of pH conditions (Figure 3, bold line). Comparing these species-specific values reveals that $k_{H_2CO_3^*}$ derived from fitting the pH-dependent data is >3-fold lower than that measured at acidic conditions alone (7.7×10^9 M^{-1} s^{-1}),[42] whereas $k_{HCO_3^-}$ and $k_{CO_3^{2-}}$ are >3-fold higher and lower, respectively, than the values reported previously (6×10^5 and 3.90×10^5 M^{-1} s^{-1}, respectively).[33,43] We hypothesize that the differences result largely from the assumption in earlier studies that the carbonate species in question was the sole quencher of e^-_{aq}. For example, the value for $k_{CO_3^{2-}}$ was measured

https://doi.org/10.1021/acs.est.2c09451
Environ. Sci. Technol. 2023, 57, 7849–7857

at pH 11.4 where CO_3^{2-} accounts for 93% of C_{T,CO_3}, but contribution of HCO_3^- to the rate constant was not considered despite this species accounting for 7% of C_{T,CO_3} and being 20-fold more reactive than CO_3^{2-}.[13,33] In addition, no mention is made of the pH at which the value for $k_{HCO_3^-}$ was measured.[43] Additional factors responsible may include differences in ionic strength or temperature. We employed a high ionic strength (0.5 M) to ensure that this parameter was constant when varying added $NaHCO_3$ (up to 0.50 M) during LFP experiments. We note that when two ions are of the same charge, their reactivity toward each other can be affected by changes in ionic strength.[44] However, the main quencher of e_{aq}^- in carbonate-containing solutions at pH < 9.3 is the neutral $CO_{2(aq)}$ species that is not expected to be strongly influenced by changing ionic strength. The insensitivity to changing ionic strength was confirmed by comparative LFP experiments conducted at low and high ionic strength conditions at pH 5.0−5.5 (Figure S5) and 8.3 (Figure S6), where $CO_{2(aq)}$ and HCO_3^- species predominate, respectively. Failure to specifically account for this variable in earlier studies may also have affected the resulting rate constant values.

Figure 3 also illustrates the relative contributions of individual carbonate species to net quenching of e_{aq}^- at different pH conditions. This shows that H_2CO_3* is the dominant quencher species at pH < 9 despite the fact that it is a minor contributor to carbonate speciation at pH > 6.35. The dominance of quenching by H_2CO_3* at pH < 9 is further highlighted by the fact that all the individual e_{aq}^- measurements at these pH conditions (40 different data points at varying concentration and pH conditions) fall onto a single Stern−Volmer-type plot when the x-axis is re-defined by the calculated concentration of H_2CO_3* (Figure S7) rather than total dissolved carbonate (C_{T,CO_3}). It is also notable that the resulting k_{app} value derived from this data set ($1.42 (\pm 0.04) \times 10^9$ M^{-1} s^{-1}) is similar to the value of $k_{H_2CO_3^*}$ obtained from fitting the pH-dependent k_{app} data set with eq 3. Nevertheless, ARP applications are most often being conducted at pH ≥ 9, where HCO_3^- is a major contributor to e_{aq}^- quenching and cannot be ignored. For example, this analysis indicates that HCO_3^- is responsible for 85% of the carbonate inhibition of PFOS degradation rates observed in Figure 1.

Reaction Mechanisms. Model fits are consistent with e_{aq}^- quenching by H_2CO_3*, HCO_3^-, and CO_3^{2-} species. H_2CO_3* is defined to include both $CO_{2(aq)}$ and H_2CO_3, which are related by the hydration/dehydration equilibrium

$$CO_{2(aq)} + H_2O \rightleftarrows H_2CO_3;\ \log K_{hyd} = -2.66 \quad (4)$$

Hence, this equilibrium is strongly shifted to the left and H_2CO_3* is dominated by $CO_{2(aq)}$ (i.e., $[CO_{2(aq)}] \approx C_{T,CO_3}$ at pH < pK_{a_1}). Earlier reports document that the reaction of $CO_{2(aq)}$ with e_{aq}^- yields the CO_2 radical anion ($CO_2^{\bullet-}$), confirmed by transient absorption spectroscopy[45]

$$CO_{2(aq)} + e_{aq}^- \rightleftarrows CO_2^{\bullet-} \quad (5)$$

While most studies to date show that increasing dissolved carbonate acts to inhibit rates of e_{aq}^- ARPs,[31,46] a recent report suggests that $CO_2^{\bullet-}$, itself, may react with more recalcitrant PFASs (e.g., perfluorobutane sulfonate).[47] However, the importance of PFAS reactions compared to other processes that rapidly consume $CO_2^{\bullet-}$, including near diffusion-limited recombination reactions, remains to be established.[21,45,48] Still, further studies of the fate and reactivity of $CO_2^{\bullet-}$ are warranted, given the likelihood for generation of this transient species during e_{aq}^-ARPs in carbonate-containing natural water matrices.

The minor contributor to H_2CO_3*, H_2CO_3, and its conjugate base HCO_3^- are Brønsted acids, where the acidic proton can react with e_{aq}^- to yield atomic hydrogen in the same manner as H_3O^+ ions[49]

$$H_3O^+ + e_{aq}^- \rightarrow H^\bullet + H_2O \quad (6)$$

$$H_2CO_3 + e_{aq}^- \rightarrow H^\bullet + HCO_3^- \quad (7)$$

$$HCO_3^- + e_{aq}^- \rightarrow H^\bullet + CO_3^{2-} \quad (8)$$

Because of its minor contribution to H_2CO_3*, we are unable to directly quantify the reactivity of H_2CO_3 with e_{aq}^-, separate from $CO_{2(aq)}$, but previous work has shown that the reactivity of different Brønsted acids varies with acid strength according to the following relationship[25]

$$\frac{k_2}{p} = G_A\left(\frac{qK_A}{p}\right)^\beta \quad (9)$$

where k_2, K_a, p, and q, respectively, represent the bimolecular rate constant for Brønsted acid reactivity with e_{aq}^-, the acid dissociation constant, the number of dissociable protons available in the acid, and the number of equivalent sites at which a proton can be attached to in the conjugate base. G_A and β are constants distinct to similar types of acids.[49] Using data presented by Maza and co-workers[25] for a series of Brønsted acids together with the pK_{a_1} of H_2CO_3 (3.45),[50] we estimate k_2 for H_2CO_3 of 4.8×10^8 M^{-1} s^{-1} (Figure S8). It is worth noting that the estimated $k_{H_2CO_3}$ is more than 4 times lower than the value determined for H_2CO_3* from fitting experimental data (2.23×10^9 M^{-1} s^{-1}), further supporting the conclusion that $CO_{2(aq)}$ is the dominant species contributing to e_{aq}^- scavenging. It is also worth noting that lower reactivity of HCO_3^- determined from model fitting (2.18×10^6 M^{-1} s^{-1}) is consistent with the Brønsted relationship described by eq 9 and similar in magnitude to the value reported for e_{aq}^- quenching by NH_4^+ (1.30×10^6 M^{-1} s^{-1}),[51] a Brønsted acid of similar strength to HCO_3^-. The fully deprotonated (CO_3^{2-}) species still reacts with e_{aq}^-, albeit very slowly. To the best of our knowledge, there are no literature reports on the product of the reaction between e_{aq}^- and CO_3^{2-} or similar polyatomic ions such as SO_3^{2-} despite rate constants being available for both.[13,33,52,53]

Relative Importance of Carbonate Species to Other Quenchers. Data presented in Figure 1 shows the importance of carbonate species as e_{aq}^- quenchers that inhibit ARP treatment of PFOS. We can more generally evaluate the importance of dissolved carbonate species relative to other quencher species expected to be abundant in natural water matrices during ARP treatment applications. The net contribution of individual quenchers can be quantified by the product of their concentration and bimolecular rate constant for reaction with e_{aq}^-, $k_i[i]$. For carbonate species, this can be formulated according to the following expression

$$k_{H_2CO_3^*}[H_2CO_3^*] + k_{HCO_3^-}[HCO_3^-] + k_{CO_3^{2-}}[CO_3^{2-}] \quad (10)$$

Other e_{aq}^- quenchers expected to be common in groundwater matrices during ARP treatments include the conjugate acid of

https://doi.org/10.1021/acs.est.2c09451
Environ. Sci. Technol. 2023, 57, 7849−7857

the sulfite photosensitizer HSO_3^- (1.2×10^8 M^{-1} s^{-1}),[25] H^+ (2.3×10^{10} M^{-1} s^{-1}),[13,54] dissolved O_2 (1.9×10^{10} M^{-1} s^{-1}),[17] and nitrate (9.7×10^9 M^{-1} s^{-1}).[13,55] It follows that total quenching of e_{aq}^- can be formulated as

$$\sum k_i[i] = k_{H_2CO_3^*}[H_2CO_3^*] + k_{HCO_3^-}[HCO_3^-] + k_{CO_3^{2-}}[CO_3^{2-}] + k_{HSO_3^-}[HSO_3^-] + k_{H^+}[H^+] + k_{O_2}[O_2] + k_{NO_3^-}[NO_3^-] \quad (11)$$

Figure 4 illustrates the predicted contribution of individual quencher species and overall quenching in solutions at varying pH conditions (Figure 4A) and varying total dissolved carbonate concentrations (Figure 4B). If we first consider matrices free of O_2 and NO_3^-, we observe strong pH dependence for the rates of quenching by different species resulting from shifts toward conjugate acid species with elevated reactivity. This trend is consistent with experimental observations that UV-sulfite treatment efficacy decreases with decreasing pH.[20,29,31] Comparing the contributions of different quencher species, it appears that carbonate and bisulfite species are the major quenchers anticipated at most conditions, with the relative contributions being dependent on their respective concentrations in the matrix of interest. For example, if the trends for 1 mM total dissolved carbonate and 10 mM sulfite are compared, simulations in Figure 4A show that carbonate quenching dominates at pH < 6.5 and >9.6, but sulfite dominates at pH conditions in between. When a lower sulfite concentration (3 mM) is used for treatment, such as in the PFOS experiments shown in Figure 1, carbonate species become the dominant quencher over the entire pH range. Investigations into UV-ARPs have often used 10 mM sulfite as a sensitizer along with 5 mM carbonate as a buffer.[23,28,56] This system is represented by the dashed line in Figure 4A, which shows that the curve representing total background quenching nearly overlaps the line for 5 mM carbonate, suggesting that carbonate alone is responsible for any pH-dependent processes involving e_{aq}^-. It is also noteworthy that H^+ contributes negligibly to e_{aq}^- quenching across the full range of pH conditions. We note that the decreases in PFOS k_{obs} were not directly proportional to the increases in added carbonate. For example, PFOS k_{obs} decreases by roughly a factor of 1.5 when increasing added carbonate from 1 to 5 mM (Figure 1). This is likely due to background levels of quenching due to non-carbonate species (e.g., bisulfite) whose effects do not scale with added carbonate. However, rudimentary analysis assuming that e_{aq}^- is the sole species reacting with PFOS would lead one to expect closer to a 1:1 correlation between degradation kinetics and quencher concentration. From this, we recognize that other species which are unaffected by dissolved carbonate could be present and react with PFOS in parallel. This warrants an in-depth analysis investigating the mechanisms and impacts of other reactive species (e.g., $SO_3^{\bullet-}$, $H^\bullet$, etc.) on contaminant transformation.

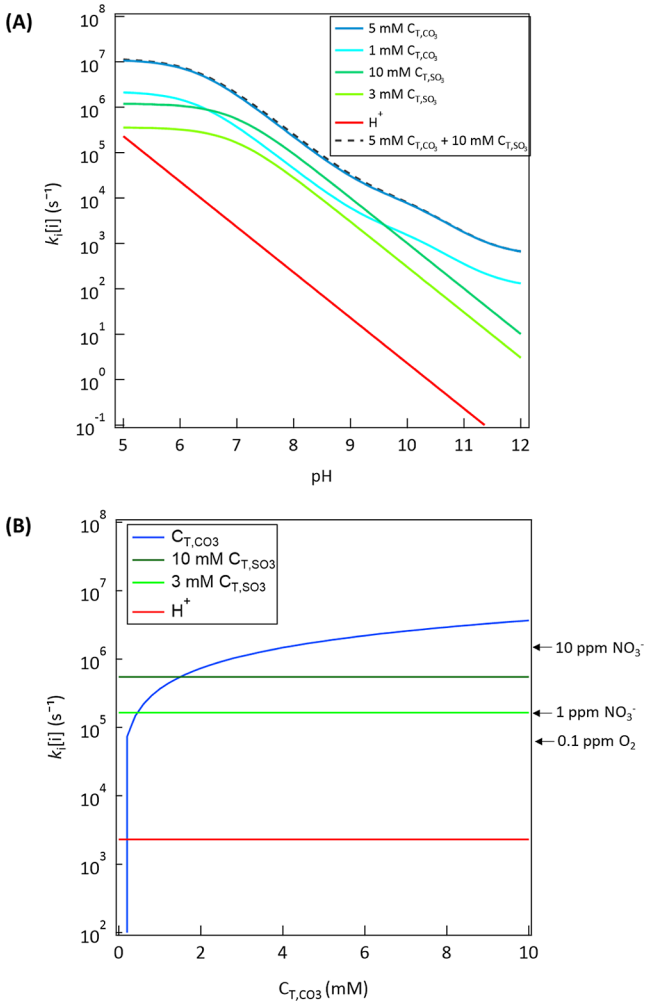

Figure 4. Simulation of the rates of e_{aq}^- scavenging by dissolved carbonate species in comparison with other common scavengers expected during groundwater treatment with UV-sulfite constructed using eq 11. Species concentrations ([i] in eq 11) were determined using Visual MINTEQ (Ver 3.1) at 20 °C and 0.05 M ionic strength. (A) Influence of pH and (B) influence of variable carbonate concentration at pH 7.0.

As shown in Figure 4B, carbonate quenching becomes important relative to anticipated sulfite quenching as total dissolved carbonate approaches millimolar levels. While the concentration of carbonate in natural waters can vary, any given source water is likely to undergo pH adjustment immediately prior to UV irradiation, and re-equilibration with atmospheric $CO_{2(g)}$ will not occur after this action is taken in a closed reactor system.[37] Thus, we believe that quantification of C_{T,CO_3} prior to treatment and inclusion of quenching by carbonate species are important within models for ARP treatment of PFAS and other recalcitrant contaminants. Simulations suggest that even at lower pH conditions relevant to natural waters (pH 6.0–8.5), H^+ is not a prevalent quencher, and therefore, if HSO_3^- quenching and dissolved carbonate quenching are minimized, it is possible for ARPs to operate efficiently without pH adjustment, which has significant practical implications.

Figure 4B also shows that quenching from dissolved O_2 and NO_3^- will be dominant when present in the matrix at elevated levels, highlighting the need to characterize these species in source waters being subjected to treatment. Although dissolved O_2 has a very high reactivity with e_{aq}^-, it is expected to be very low in concentration during UV-sulfite treatment applications because sulfite is an effective scavenger of O_2 and suppresses its concentration.[12] In fact, recent studies show that there is little benefit to actively deoxygenating solutions prior to UV-sulfite treatment since the sensitizer effectively suppresses dissolved oxygen concentrations and eliminates scavenging of e_{aq}^-

https://doi.org/10.1021/acs.est.2c09451
Environ. Sci. Technol. 2023, 57, 7849−7857

generated upon UV irradiation.[36] Still, this is an issue to be aware of when applying other ARPs. Nitrate is also known to be a strong scavenger of e^-_{aq}, so nitrate-contaminated water matrices will require denitrification before applying ARPs to treat less reactive contaminants like PFASs. The ARPs themselves can remove the nitrate, but the additional e^-_{aq} demand of the matrix needs to be accounted for in treatment system design. These findings provide critical insights into the operative mechanisms responsible for poor performance of ARPs often observed at lower pH conditions. They also provide mechanistic support for the recent design recommendations to adjust pH conditions prior to UV-sulfite treatment.[23] Ultimately, quantitative information on background scavenging of source water matrices, such as those provided here, provides critical information needed to improve predictions and design of ARP technologies for treatment of recalcitrant micropollutants such as PFASs. Because k_2 values for e^-_{aq} reactions with many common water constituents are known,[13] quantitative analysis of their impact on UV-ARPs can be described using the tools presented here. We note that the development of a comprehensive kinetic model naturally follows the results of this work which will be reported in a follow-up study focusing on the prediction of PFAS degradation during UV-sulfite treatment in diverse environments.

■ ASSOCIATED CONTENT

Supporting Information

The Supporting Information is available free of charge at https://pubs.acs.org/doi/10.1021/acs.est.2c09451.

List of chemicals, detailed solution preparation, experimental methods, additional data, LFP traces, and Stern−Volmer plots (PDF)

■ AUTHOR INFORMATION

Corresponding Authors

Shubham Vyas − *Department of Chemistry, Colorado School of Mines, Golden, Colorado 80401, United States;* orcid.org/0000-0002-5849-8919; Email: svyas@mines.edu

Timothy J. Strathmann − *Department of Civil and Environmental Engineering, Colorado School of Mines, Golden, Colorado 80401, United States;* orcid.org/0000-0002-7299-3115; Email: strthmnn@mines.edu

Authors

Camille K. Amador − *Department of Civil and Environmental Engineering, Colorado School of Mines, Golden, Colorado 80401, United States; Department of Chemistry, Colorado School of Mines, Golden, Colorado 80401, United States;* orcid.org/0000-0002-6142-9738

Haden Cavalli − *Department of Chemistry, Colorado School of Mines, Golden, Colorado 80401, United States*

Raul Tenorio − *Department of Civil and Environmental Engineering, Colorado School of Mines, Golden, Colorado 80401, United States;* Present Address: Haley & Aldrich, 400 E Van Buren St #545, Phoenix, AZ 85004, United States; orcid.org/0000-0001-9788-7100

Hanna Tetu − *Department of Chemistry, Colorado School of Mines, Golden, Colorado 80401, United States*

Christopher P. Higgins − *Department of Civil and Environmental Engineering, Colorado School of Mines, Golden, Colorado 80401, United States;* orcid.org/0000-0001-6220-8673

Complete contact information is available at: https://pubs.acs.org/10.1021/acs.est.2c09451

Notes

The authors declare no competing financial interest.

■ ACKNOWLEDGMENTS

This work was financially supported by the National Science Foundation (CHE-1807739 and CHE-2109210). We thank Nicholas Gonda and Prof. Bettina Voelker for helpful discussions about carbonic acid chemistry and Dr. Shilai Hao, Dr. Charlie Liu, and Anderson Ellis for assistance with LC−MS/MS analysis. Glory Russell-Parks is also acknowledged for providing necessary laboratory supplies.

■ REFERENCES

(1) Vellanki, B. P.; Batchelor, B.; Abdel-Wahab, A. Advanced Reduction Processes: A New Class of Treatment Processes. *Environ. Eng. Sci.* **2013**, *30*, 264−271.

(2) Gu, Y.; Dong, W.; Luo, C.; Liu, T. Efficient Reductive Decomposition of Perfluorooctanesulfonate in a High Photon Flux UV/Sulfite System. *Environ. Sci. Technol.* **2016**, *50*, 10554−10561.

(3) Bao, Y.; Huang, J.; Cagnetta, G.; Yu, G. Removal of F−53B as PFOS Alternative in Chrome Plating Wastewater by UV/Sulfite Reduction. *Water Res.* **2019**, *163*, 114907.

(4) Liu, X.; Vellanki, B. P.; Batchelor, B.; Abdel-Wahab, A. Degradation of 1,2-Dichloroethane with Advanced Reduction Processes (ARPs): Effects of Process Variables and Mechanisms. *Chem. Eng. J.* **2014**, *237*, 300−307.

(5) Vellanki, B. P.; Batchelor, B. Perchlorate Reduction by the Sulfite/Ultraviolet Light Advanced Reduction Process. *J. Hazard. Mater.* **2013**, *262*, 348−356.

(6) Jung, B.; Nicola, R.; Batchelor, B.; Abdel-Wahab, A. Effect of Low- and Medium-Pressure Hg UV Irradiation on Bromate Removal in Advanced Reduction Process. *Chemosphere* **2014**, *117*, 663−672.

(7) Liu, X.; Zhang, T.; Shao, Y. Aqueous Bromate Reduction by UV Activation of Sulfite: Aqueous Bromate Reduction by UV Activation of Sulfite. *Clean: Soil, Air, Water* **2014**, *42*, 1370−1375.

(8) Botlaguduru, V. S. V.; Batchelor, B.; Abdel-Wahab, A. Application of UV−Sulfite Advanced Reduction Process to Bromate Removal. *J. Water Process Eng.* **2015**, *5*, 76−82.

(9) Gu, Y.; Liu, T.; Wang, H.; Han, H.; Dong, W. Hydrated Electron Based Decomposition of Perfluorooctane Sulfonate (PFOS) in the VUV/Sulfite System. *Sci. Total Environ.* **2017**, *607−608*, 541−548.

(10) Marcus, R. A. Theory of Electron-Transfer Reaction Rates of Solvated Electrons. *J. Chem. Phys.* **1965**, *43*, 3477−3489.

(11) Baxendale, J. H. Addendum: Redox Potential and Hydration Energy of the Hydrated Electron. *Radiat. Res., Suppl.* **1964**, *4*, 139.

(12) Hayon, E.; Treinin, A.; Wilf, J. Electronic Spectra, Photochemistry, and Autoxidation Mechanism of the Sulfite-Bisulfite-Pyrosulfite Systems. SO2-SO3-SO4-and SO5- Radicals. *J. Am. Chem. Soc.* **1972**, *94*, 47−57.

(13) Buxton, G. V.; Greenstock, C. L.; Helman, W. P.; Ross, A. B. Critical Review of Rate Constants for Reactions of Hydrated Electrons, Hydrogen Atoms and Hydroxyl Radicals (·OH/·O $^-$ in Aqueous Solution. *J. Phys. Chem. Ref. Data* **1988**, *17*, 513−886.

(14) Sathasivan, A.; Herath, B. S.; Senevirathna, S. T. M. L. D.; Kastl, G. Dechlorination in Wastewater Treatment Processes. In *Current Developments in Biotechnology and Bioengineering*; Elsevier, 2017, pp 359−380.

(15) Lapointe, F.; Wolf, M.; Campen, R. K.; Tong, Y. Probing the Birth and Ultrafast Dynamics of Hydrated Electrons at the Gold/Liquid Water Interface via an Optoelectronic Approach. *J. Am. Chem. Soc.* **2020**, *142*, 18619−18627.

(16) Abel, B.; Buck, U.; Sobolewski, A. L.; Domcke, W. On the Nature and Signatures of the Solvated Electron in Water. *Phys. Chem. Chem. Phys.* **2012**, *14*, 22−34.
(17) Milosavljevic, B. H.; Micic, O. I. Solvated Electron Reactions in Water-Alcohol Solutions. *J. Phys. Chem.* **1978**, *82*, 1359−1362.
(18) Gonzalez, M.; Oliveros, E.; Worner, M.; Braun, A. Vacuum-Ultraviolet Photolysis of Aqueous Reaction Systems. *J. Photochem. Photobiol., C* **2004**, *5*, 225−246.
(19) Barat, F.; Gilles, L.; Hickel, B.; Lesigne, B. Effect of the Dielectric Constant on the Reactivity of the Solvated Electron. *J. Phys. Chem.* **1973**, *77*, 1711−1715.
(20) Qu, Y.; Zhang, C.-J.; Chen, P.; Zhou, Q.; Zhang, W.-X. Effect of Initial Solution PH on Photo-Induced Reductive Decomposition of Perfluorooctanoic Acid. *Chemosphere* **2014**, *107*, 218−223.
(21) Cui, J.; Gao, P.; Deng, Y. Destruction of Per- and Polyfluoroalkyl Substances (PFAS) with Advanced Reduction Processes (ARPs): A Critical Review. *Environ. Sci. Technol.* **2020**, *54*, 3752−3766.
(22) Fennell, B. D.; Mezyk, S. P.; McKay, G. Critical Review of UV-Advanced Reduction Processes for the Treatment of Chemical Contaminants in Water. *ACS Environ. Au* **2022**, *2*, 178−205.
(23) Bentel, M. J.; Liu, Z.; Yu, Y.; Gao, J.; Men, Y.; Liu, J. Enhanced Degradation of Perfluorocarboxylic Acids (PFCAs) by UV/Sulfite Treatment: Reaction Mechanisms and System Efficiencies at PH 12. *Environ. Sci. Technol. Lett.* **2020**, *7*, 351−357.
(24) Amador, C. K.; Van Hoomissen, D. J.; Liu, J.; Strathmann, T. J.; Vyas, S. Ultra-Short Chain Fluorocarboxylates Exhibit Wide Ranging Reactivity with Hydrated Electrons. *Chemosphere* **2023**, *311*, 136918.
(25) Maza, W. A.; Breslin, V. M.; Plymale, N. T.; DeSario, P. A.; Epshteyn, A.; Owrutsky, J. C.; Pate, B. B. Nanosecond Transient Absorption Studies of the PH-Dependent Hydrated Electron Quenching by HSO_3^-. *Photochem. Photobiol. Sci.* **2019**, *18*, 1526−1532.
(26) Levin, P. P.; Brzhevskaya, O. N.; Nedelina, O. S. Kinetics of Hydrated Electron Reactions with Phosphate Anions: A Laser Photolysis Study. *Russ. Chem. Bull.* **2007**, *56*, 1325−1328.
(27) Dogliotti, L.; Hayon, E. Flash Photolysis Study of Sulfite, Thiocyanate, and Thiosulfate Ions in Solution. *J. Phys. Chem.* **1968**, *72*, 1800−1807.
(28) Tenorio, R.; Liu, J.; Xiao, X.; Maizel, A.; Higgins, C. P.; Schaefer, C. E.; Strathmann, T. J. Destruction of Per- and Polyfluoroalkyl Substances (PFASs) in Aqueous Film-Forming Foam (AFFF) with UV-Sulfite Photoreductive Treatment. *Environ. Sci. Technol.* **2020**, *54*, 6957−6967.
(29) Bentel, M. J.; Yu, Y.; Xu, L.; Li, Z.; Wong, B. M.; Men, Y.; Liu, J. Defluorination of Per- and Polyfluoroalkyl Substances (PFASs) with Hydrated Electrons: Structural Dependence and Implications to PFAS Remediation and Management. *Environ. Sci. Technol.* **2019**, *53*, 3718−3728.
(30) Liu, Z.; Bentel, M. J.; Yu, Y.; Ren, C.; Gao, J.; Pulikkal, V. F.; Sun, M.; Men, Y.; Liu, J. Near-Quantitative Defluorination of Perfluorinated and Fluorotelomer Carboxylates and Sulfonates with Integrated Oxidation and Reduction. *Environ. Sci. Technol.* **2021**, *55*, 7052−7062.
(31) Ren, Z.; Bergmann, U.; Leiviskä, T. Reductive Degradation of Perfluorooctanoic Acid in Complex Water Matrices by Using the UV/Sulfite Process. *Water Res.* **2021**, *205*, 117676.
(32) Thomas, J. K.; Gordon, S.; Hart, E. J. The Rates of Reaction of the Hydrated Electron in Aqueous Inorganic Solutions [1]. *J. Phys. Chem.* **1964**, *68*, 1524−1527.
(33) Nash, K.; Mulac, W.; Noon, M.; Fried, S.; Sullivan, J. C. Pulse Radiolysis Studies of U(VI) Complexes in Aqueous Media. *J. Inorg. Nucl. Chem.* **1981**, *43*, 897−899.
(34) Gordon, S.; Hart, E. J.; Matheson, M. S.; Rabani, J.; Thomas, J. K. Reactions of the Hydrated Electron. *Discuss. Faraday Soc.* **1963**, *36*, 193.
(35) Ellis, A. C.; Liu, C. J.; Fang, Y.; Boyer, T. H.; Schaefer, C. E.; Higgins, C. P.; Strathmann, T. J. Pilot Study Comparison of Regenerable and Emerging Single-Use Anion Exchange Resins for Treatment of Groundwater Contaminated by per- and Polyfluoroalkyl Substances (PFASs). *Water Res.* **2022**, *223*, 119019.
(36) Liu, C. J.; McKay, G.; Jiang, D.; Tenorio, R.; Cath, J. T.; Amador, C.; Murray, C. C.; Brown, J. B.; Wright, H. B.; Schaefer, C.; Higgins, C. P.; Bellona, C.; Strathmann, T. J. Pilot-Scale Field Demonstration of a Hybrid Nanofiltration and UV-Sulfite Treatment Train for Groundwater Contaminated by Per- and Polyfluoroalkyl Substances (PFASs). *Water Res.* **2021**, *205*, 117677.
(37) Lisovskaya, A.; Bartels, D. M. Reduction of CO2 by Hydrated Electrons in High Temperature Water. *Radiat. Phys. Chem.* **2019**, *158*, 61−63.
(38) Abramczyk, H.; Werner, B.; Kroh, J. Absorption Spectra of the Solvated Electron in Hydrocarbons. *J. Phys. Chem.* **1992**, *96*, 9674−9677.
(39) Sauer, M. C.; Crowell, R. A.; Shkrob, I. A. Electron Photodetachment from Aqueous Anions. 1. Quantum Yields for Generation of Hydrated Electron by 193 and 248 Nm Laser Photoexcitation of Miscellaneous Inorganic Anions. *J. Phys. Chem. A* **2004**, *108*, 5490−5502.
(40) Huang, L.; Dong, W.; Hou, H. Investigation of the Reactivity of Hydrated Electron toward Perfluorinated Carboxylates by Laser Flash Photolysis. *Chem. Phys. Lett.* **2007**, *436*, 124−128.
(41) Song, Z.; Tang, H.; Wang, N.; Zhu, L. Reductive Defluorination of Perfluorooctanoic Acid by Hydrated Electrons in a Sulfite-Mediated UV Photochemical System. *J. Hazard. Mater.* **2013**, *262*, 332−338.
(42) Getoff, N. Possibilities on the Radiation-Induced Incorporation of CO2 and CO into Organic Compounds☆. *Int. J. Hydrogen Energy* **1994**, *19*, 667−672.
(43) Hentz, R. R.; Farhataziz; Milner, D. J.; Burton, M. γ Radiolysis of Liquids at High Pressures. III. Aqueous Solutions of Sodium Bicarbonate. *J. Chem. Phys.* **1967**, *47*, 374−377.
(44) Arnaut, L.; Burrows, H. *Chemical Kinetics*; Elsevier, 2007.
(45) Neta, P.; Simic, M.; Hayon, E. Pulse Radiolysis of Aliphatic Acids in Aqueous Solutions. I. Simple Monocarboxylic Acids. *J. Phys. Chem.* **1969**, *73*, 4207−4213.
(46) Fennell, B. D.; Odorisio, A.; McKay, G. Quantifying Hydrated Electron Transformation Kinetics in UV-Advanced Reduction Processes Using the $R_{e-,UV}$ Method. *Environ. Sci. Technol.* **2022**, *56*, 10329−10338.
(47) Jiang, Z.; Adjei, D.; Denisov, S. A.; Mostafavi, M.; Ma, J. Transient Kinetics of Short-Chain Perfluoroalkyl Sulfonate with Radiolytic Reducing Species. *Environ. Sci. Technol. Lett.* **2022**, *10*, 59.
(48) Li, X.; Fang, J.; Liu, G.; Zhang, S.; Pan, B.; Ma, J. Kinetics and Efficiency of the Hydrated Electron-Induced Dehalogenation by the Sulfite/UV Process. *Water Res.* **2014**, *62*, 220−228.
(49) Jortner, J.; Ottolenghi, M.; Rabani, J.; Stein, G. Conversion of Solvated Electrons into Hydrogen Atoms in the Photo- and Radiation Chemistry of Aqueous Solutions. *J. Chem. Phys.* **1962**, *37*, 2488−2495.
(50) Adamczyk, K.; Prémont-Schwarz, M.; Pines, D.; Pines, E.; Nibbering, E. T. J. Real-Time Observation of Carbonic Acid Formation in Aqueous Solution. *Science* **2009**, *326*, 1690−1694.
(51) Hart, E. J.; Gordon, S.; Thomas, J. K. Rate Constants of Hydrated Electron Reactions with Organic Compounds [1]. *J. Phys. Chem.* **1964**, *68*, 1271−1274.
(52) Zagorski, Z. P.; Sehested, K.; Nielsen, S. O. Pulse Radiolysis of Aqueous Alkaline Sulfite Solutions. *J. Phys. Chem.* **1971**, *75*, 3510−3517.
(53) Anbar, M. The Reactions of Hydrated Electrons with Organic Compounds. *Adv. Phys. Org. Chem.* **1969**, *7*, 115−151.
(54) *Solvated Electron*; Hart, E. J., Ed.; *Advances in Chemistry*; American Chemical Society: Washington, D.C., 1965; Vol. *50*.
(55) Wallace, S. C.; Thomas, J. K. Reactions in Micellar Systems. *Radiat. Res.* **1973**, *54*, 49.
(56) Liu, Z.; Chen, Z.; Gao, J.; Yu, Y.; Men, Y.; Gu, C.; Liu, J. Accelerated Degradation of Perfluorosulfonates and Perfluorocarboxylates by UV/Sulfite + Iodide: Reaction Mechanisms and System Efficiencies. *Environ. Sci. Technol.* **2022**, *56*, 3699−3709.

https://doi.org/10.1021/acs.est.2c09451
Environ. Sci. Technol. 2023, 57, 7849−7857

Supporting Information

for

Influence of Carbonate Speciation on Hydrated Electron Treatment Processes

Camille K. Amador,[1,2] Haden Cavalli,[2] Raul Tenorio,[1,3] Hanna Tetu,[2] Christopher P. Higgins,[1] Shubham Vyas,[2*] and Timothy J. Strathmann [1]*

[1]Department of Civil and Environmental Engineering, Colorado School of Mines, Golden, CO, 80401, USA

[2]Department of Chemistry, Colorado School of Mines, Golden, CO, 80401, USA

[3]Haley & Aldrich, 400 E Van Buren St #545, Phoenix, AZ 85004, USA (Current Affiliation)

*strthmnn@mines.edu

Contents

S1. Methods

S1.1 Reagents.

Constant irradiation and LFP experiments. All chemicals were used as received without further purification. Potassium ferricyanide (100.2%), sodium chloride (100.5%), sodium hydroxide (97.5%), and sodium bicarbonate (99.7%-100.3%) were purchased from Fisher Chemical. Sodium borate, tetra (99.5–101.5%) was purchased from Baker & Adamson. Potassium ferrocyanide (101.3%) was purchased from J.T. Baker. Hydrochloric acid (36.5%-38% was purchased from Macron Fine Chemicals. Sodium sulfite (≥ 98%), and perfluorooctane sulfonate (98%) were purchased from Sigma-Aldrich.

Deoxygenated water was used to prepare all solutions inside an anaerobic glovebox (Coy Labs) to eliminate scavenging of e^-_{aq} by dissolved oxygen, unless otherwise noted. Briefly, this was prepared by boiling nanopure water for 3 h while stirring and sparging with $N_{2(g)}$. After sparging, the deoxygenated water was transferred into the glovebox and allowed to equilibrate with the atmosphere (97% $N_{2(g)}$, 3% $H_{2(g)}$) overnight while stirring.

LC-QqQ-MS analysis. Optima® HPLC-grade ammonium hydroxide solution (AmOH), Optima® HPLC-grade ammonium acetate (AmAc). Optima® HPLC-grade water, and Optima® HPLC-grade methanol were purchased from Fischer Scientific.

S1.2 Method for constant UV-sulfite irradiation experiments and analysis.

Photoreactions. Stock solutions for constant irradiation experiments are summarized in **Table S1**. Final reaction volume was 575 ml for all constant irradiation experiments, and pH was adjusted to pH 10 using 1 M NaOH and buffered using 5 mM borate. Borate and carbonate solutions (570 ml total in nanopure water) were added to the reactors and deoxygenated by sparging $N_{2(g)}$ into the systems while stirring for 1 h prior to the reaction. In addition, UV lamps were warmed up for 15 min prior to initiating photoreactions. Solutions of sulfite and PFOS were prepared in vials within the glovebox (~5 ml total), then removed from the chamber and immediately spiked into the photoreactor using stainless-steel syringes to initiate the photoreaction. 5 ml aliquots were then collected from the reactors at predetermined timepoints using the stainless-steel syringes and were stored at 4 °C until analysis. Syringes were rinsed with 25 ml nanopure water in between samples. Solution pH was re-measured after the reaction was completed to evaluate any pH drift during experiments. While there is a potential for side reactions to occur, their effects would be consistent across each UV photoreaction since the only variable changing between experiments is added carbonate ($C_{T,CO3}$). In addition, effects from the buffer (sodium tetraborate) are likely to be negligible because it is not a e^-_{aq} quencher and absorbs negligibly at 254 nm.[1,2] Moreover, the photolysis products of sulfite are e^-_{aq} and $SO_3^{\cdot-}$ (sulfite radical), which is a mild oxidant and poor reductant and therefore its role in PFOS transformation will be insignificant compared to e^-_{aq}.[3]

LC-QqQ-MS sample preparation and analysis. Reaction samples were diluted to fall within the range of the calibration curve (0.1 – 7.5 ug/L) PFOS using 80:20 MeOH:H_2O and diluted AmOH. Double blanks (80:20 MeOH and diluted AmOH) were injected throughout the analysis to verify no contamination. Calibration standards were matrix-matched to the diluted reaction samples to ensure background levels were consistent between the standards and samples (67 μM sulfite and 33 μM borate after dilution). Lab blanks were injected at the beginning of analysis to ensure matrix components did not contain target compound (PFOS). 100 μL of each sample and calibration standard was injected using a CTC PAL autosampler onto an Agilent 1200 Series LC high-pressure liquid chromatography (HPLC) system set up with a guard column (SecurityGuard, Phenomenex), two guard cartridges (ZORBAX Diol, Agilent, 6 μm, 4.6 × 12.5 mm), and a Gemini C18 analytical column (3 mm × 100 mm, 5 μm; Phenomenex). Column oven

temperature was fixed at 40 °C. The mobile phases consisted of 20 mM AmAc (mobile phase A) and methanol (mobile phase B). A gradient method was used, as described in **Table S2**.

S1.3 LFP solution preparation. All stock solutions (**Table S1**) and reaction samples were prepared in the glovebox using deoxygenated water (prepared as described above). Unless otherwise noted, reaction samples were first prepared in 5 × 50 ml centrifuge tubes with an increasing amount of bicarbonate quencher along with 40 μM $K_4Fe(CN)_6$, 10 μM $K_3Fe(CN)_6$, and NaCl as an electrolyte to balance ionic strength at ~0.5 M. 1 M NaOH and 1 M HCl were used to adjust pH to the desired condition. Final volume of each reaction sample was 20 ml, and 3 × 2.75 ml aliquots of the solutions were transferred to 15 separate cuvettes for triplicate measurement. Cuvettes were then covered with parafilm and immediately run in LFP experiments after removing from the glovebox. Additions of bicarbonate quencher were 0-0.5 M for pH conditions 12.0 to 7.3, 0.0-0.05 M for pH 6.8 to 6.3, and finally 0-0.01 M for pH 5.8. Various amounts of carbonate were added based on pH condition because at the highly alkaline conditions, the quenching reaction was slow and required high quencher concentrations to observe e^-_{aq} lifetime changes, while the opposite is true at moderate and low pH values. To ensure pH was constant during reactions, pH was measured after flash photolysis by pooling solutions from the three replicate cuvettes for a total volume of 8.5 ml. Although high concentrations of carbonate were required for Stern-Volmer analysis at high pH conditions, its presence is not expected to alter e^-_{aq} concentration because the $K_4Fe(CN)_6$ sensitizer used for laser flash photolysis experiments has a very high molar extinction coefficient and quantum yield of 4480 M^{-1} cm^{-1} and 0.674, respectively.[4,5] Meanwhile, bicarbonate, the dominant species at $6.3 < pH < 10.3$ was found to have a very low extinction coefficient of 0.0206 M^{-1} cm^{-1} at the same wavelength.[4] In addition, Hart and Boag report an insignificant difference in in the absorbance spectrum of e^-_{aq} in the presence of Na_2CO_3 in anoxic water.[6] Indeed, minimal changes were measured in UV absorbance at elevated carbonate concentrations (**Figure S1**). Moreover, the maximum absorbance standard deviations in the e^-_{aq} transient traces for the conditions requiring ~0.5 M $C_{T,CO3}$ (i.e., pH 7.3-9.8) were all < 12% of the averages when comparing the various $C_{T,CO3}$ concentrations (see Figure S9e-k).

CO_2 saturated solution was prepared from the deoxygenated water in the glovebox by bubbling $CO_{2(g)}$ at 1 atm for 14 h into a 250 ml sidearm flask affixed with a holed stopper to ensure that CO_2 did not saturate the glovebox atmosphere. Gas was allowed to exit the flask through a tube secured to the sidearm that led outside the glovebox. This solution was used to measure the bimolecular rate constant of $H_2CO_3^*$ (which consists of mostly $CO_{2(aq)}$ and some H_2CO_3) in acidic conditions. The pH of the samples prepared in this manner spanned from 5.0-5.5 with pH decreasing with increasing $CO_{2(aq)}$ concentration.. For this experiment, to ensure $CO_{2(aq)}$ did not partition into the gas phase, samples were made directly in the quartz cuvettes at a total volume of 3.5 ml to minimize headspace. Addition of $CO_{2(aq)}$ quencher for this experiment was 0-1.36 mM, while other conditions were identical to those above (40 μM $K_4Fe(CN)_6$, 10 μM $K_3Fe(CN)_6$, and NaCl for ionic strength balance at 0.5 M). pH was measured after flash photolysis by pooling solutions from the three replicate cuvettes for a total volume of 10.5 ml.

Table S1. Chemical concentrations of stock solutions used in constant irradiation (C.I.) and laser flash photolysis (LFP) experiments.

Stock solution	Component	Experiment type	Deoxygenated?	Concentration
Borate buffer	$Na_2B_4O_7 \bullet 10\ H_2O$	C.I.	No	0.05 M
Sodium sulfite	Na_2SO_3	C.I.	Yes	1.64 M
NaOH	NaOH	C.I.	No	1 M
HCl	HCl	C.I.	No	1 M
PFOS	PFOS	C.I.	Yes	172.5 mg/L
Sodium bicarbonate	$NaHCO_3$	C.I.	No	0.96 M
Salt offset	NaCl	LFP	Yes	1 M
Potassium ferricyanide	$K_3Fe(CN)_6$	LFP	Yes	5 mM
Potassium ferrocyanide	$K_4Fe(CN)_6 \bullet 3H_2O$	LFP	Yes	10 mM
NaOH	NaOH	LFP	Yes	1 M
HCl	HCl	LFP	Yes	1 M
Sodium bicarbonate	$NaHCO_3$	LFP	Yes	0.5 M
$CO_{2(aq)}$ saturated solution	$CO_{2(aq)}$	LFP	Yes	31.8 mM[a]

[a]Solution was saturated with CO_2 at room temperature giving a CO_2 concentration of 0.0318 (Henry's law constant K_H = 0.034 mol/kgBar).[7]

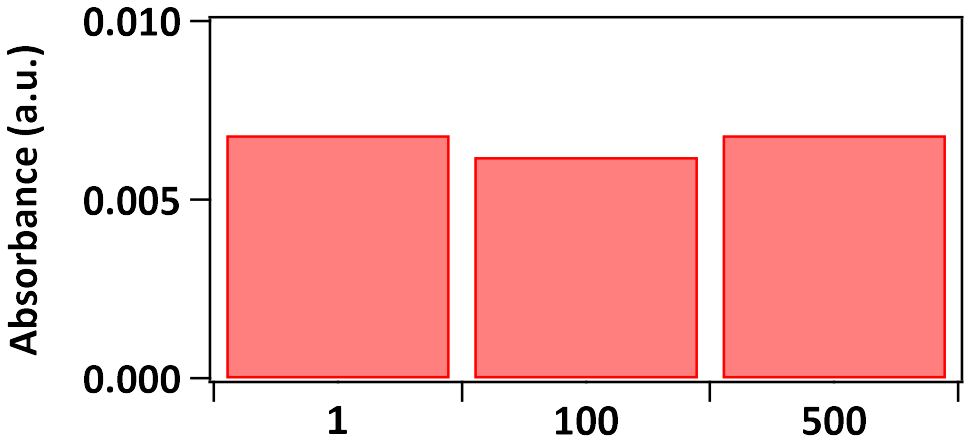

Figure S1. Absorbance of solutions containing varying concentrations of added carbonate at 0.5 mM in nanopure water.

Table S2. Gradient pump method used for PFOS analysis on LC-QqQ-MS

Total time (min)	Flow rate (µl/min)	A (%)	B (%)
0	600	90	10
0.5	600	90	10
1	600	50	50
8.5	600	1	99
10	600	1	99

S2. Additional Data

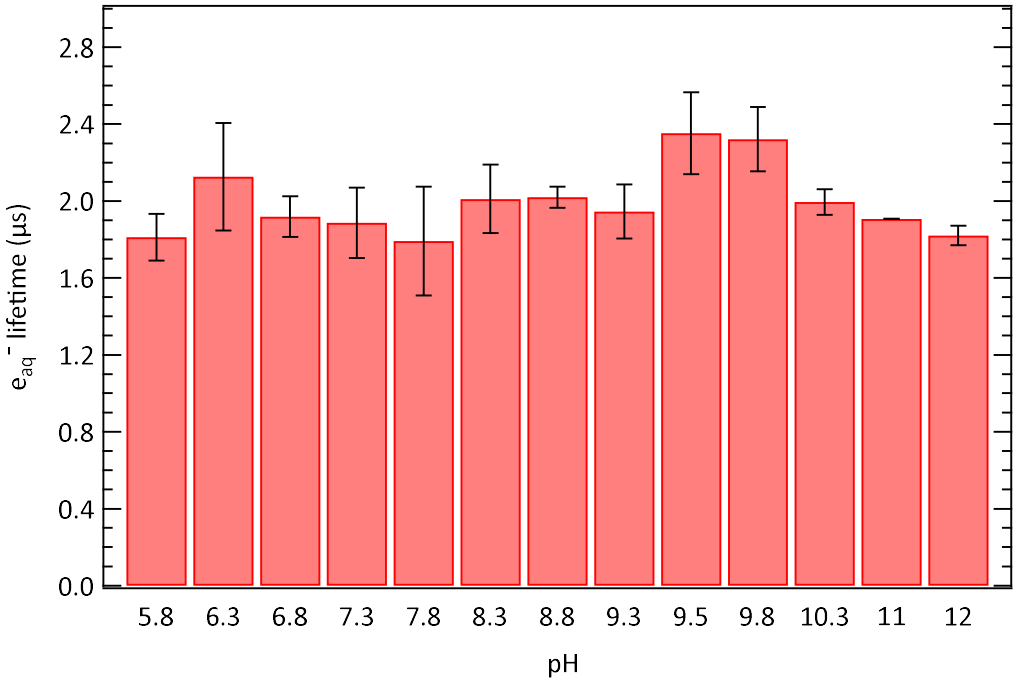

Figure S2. Hydrated electron lifetimes measured at various pH conditions in the absence of added carbonate. Reaction conditions are listed in Table 1.

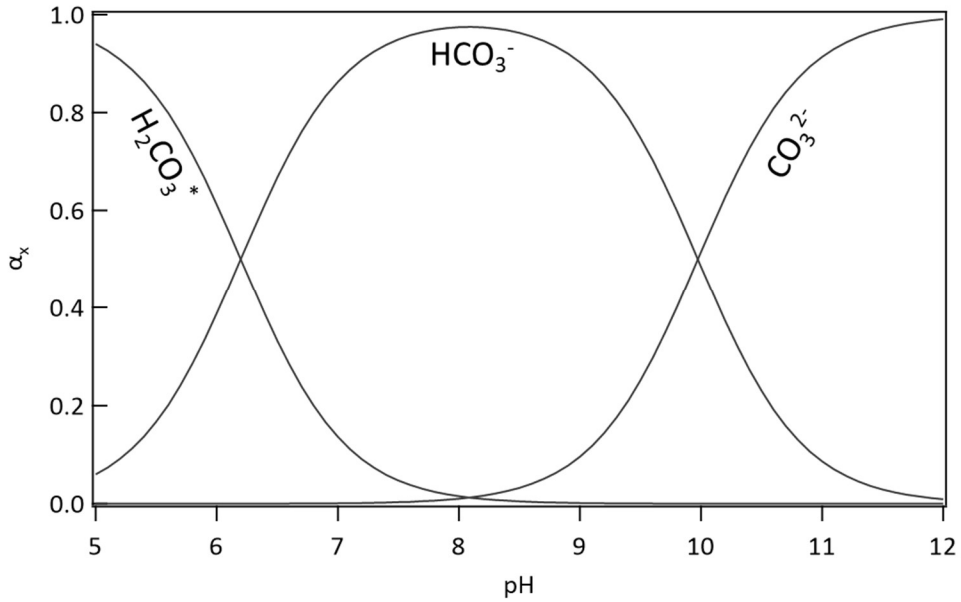

Figure S3. Speciation diagram of dissolved carbonate at I.S. = 0.5 M and 20 °C calculated using Visual MINTEQ.

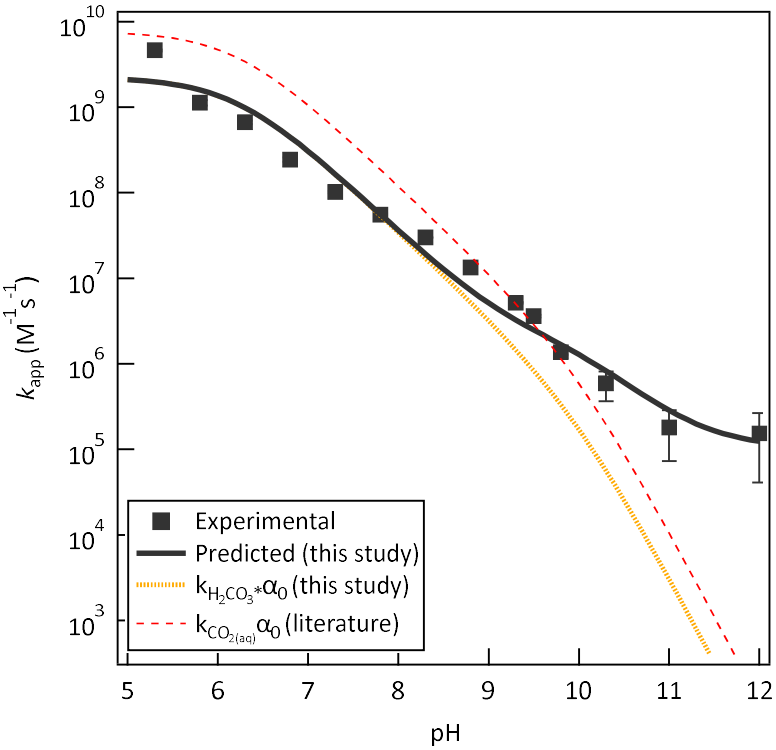

Figure S4. Effect of pH on measured (black squares) and model-predicted apparent rate constants for e^-_{aq} reaction with dissolved carbonate species. Simulated contributions of $H_2CO_3^*$ using the value from this study (beveled orange line) and the value for $CO_{2(aq)}$ determined at acidic conditions from Getoff et al.[8] Overall quenching using values from this study is shown as a bold black line.

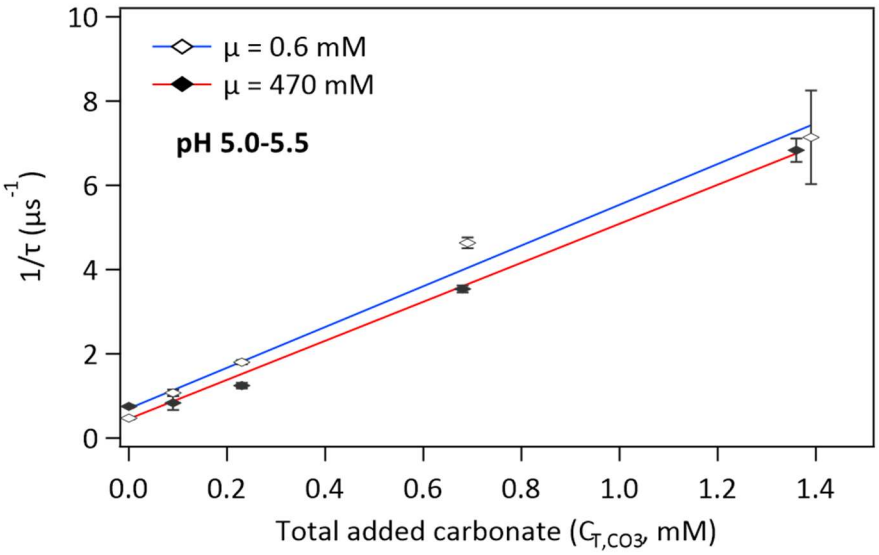

Figure S5. Stern-Volmer plots at high (red) and low (blue) ionic strength. The measured k_{app} value at 0.6 mM ionic strength is comparable to that derived at 470 mM: $4.84 \pm 0.28 \times 10^9$ and $4.63 \pm 0.13 \times 10^9$ M^{-1} s^{-1}, respectively.

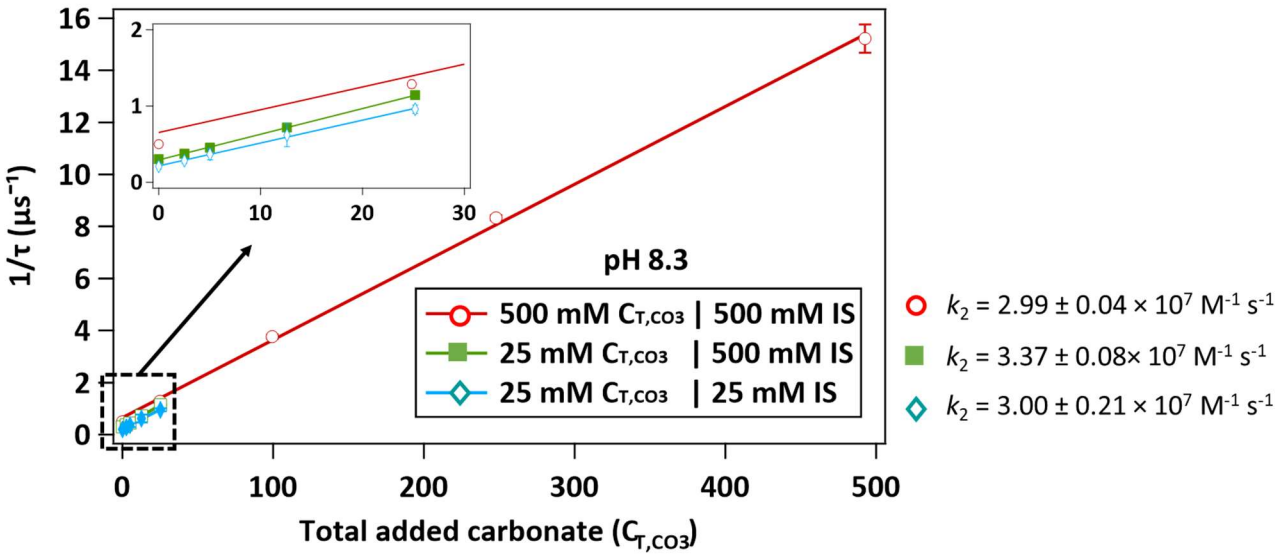

Figure S6. Stern-Volmer plots conducted at various $C_{T,CO3}$ and ionic strength conditions at pH 8.3.

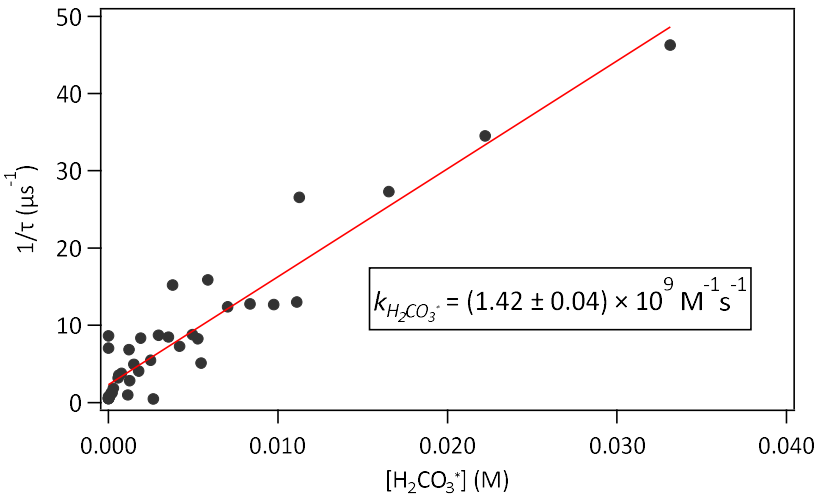

Figure S7. Stern-Volmer plot for all LFP measurements at pH conditions < 9 where e^-_{aq} lifetimes are plotted as a function of $H_2CO_3^*$. Species concentrations were calculated using Visual MINTEQ.

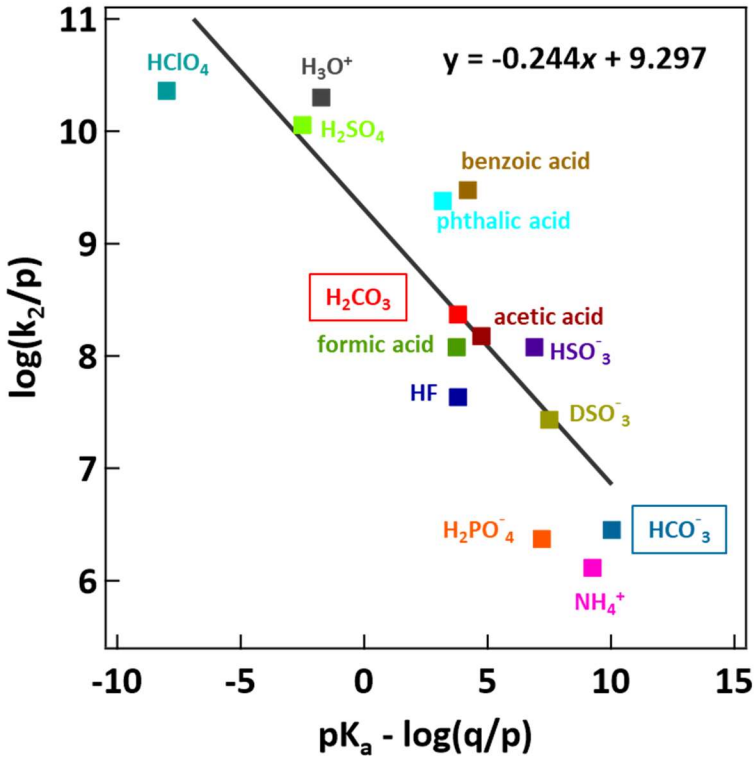

Figure S8. Bronsted law for the conversion of e^-_{aq} to H· by HCO_3^- (from this study), as well as values for other protonated acids. Solid black line represents the line of best fit determined from linear regression used to predict k_{H2CO3} (pK_a = 3.5, red symbol). Refs[9–12]. Datapoint for HCO_3^- (teal square) was determined using the k_{HCO3-} value from this study (2.18 × 10^6 M^{-1} s^{-1}).

S3. LFP transient traces and Stern-Volmer plots

LFP kinetic traces and SV-plots for various pH conditions.

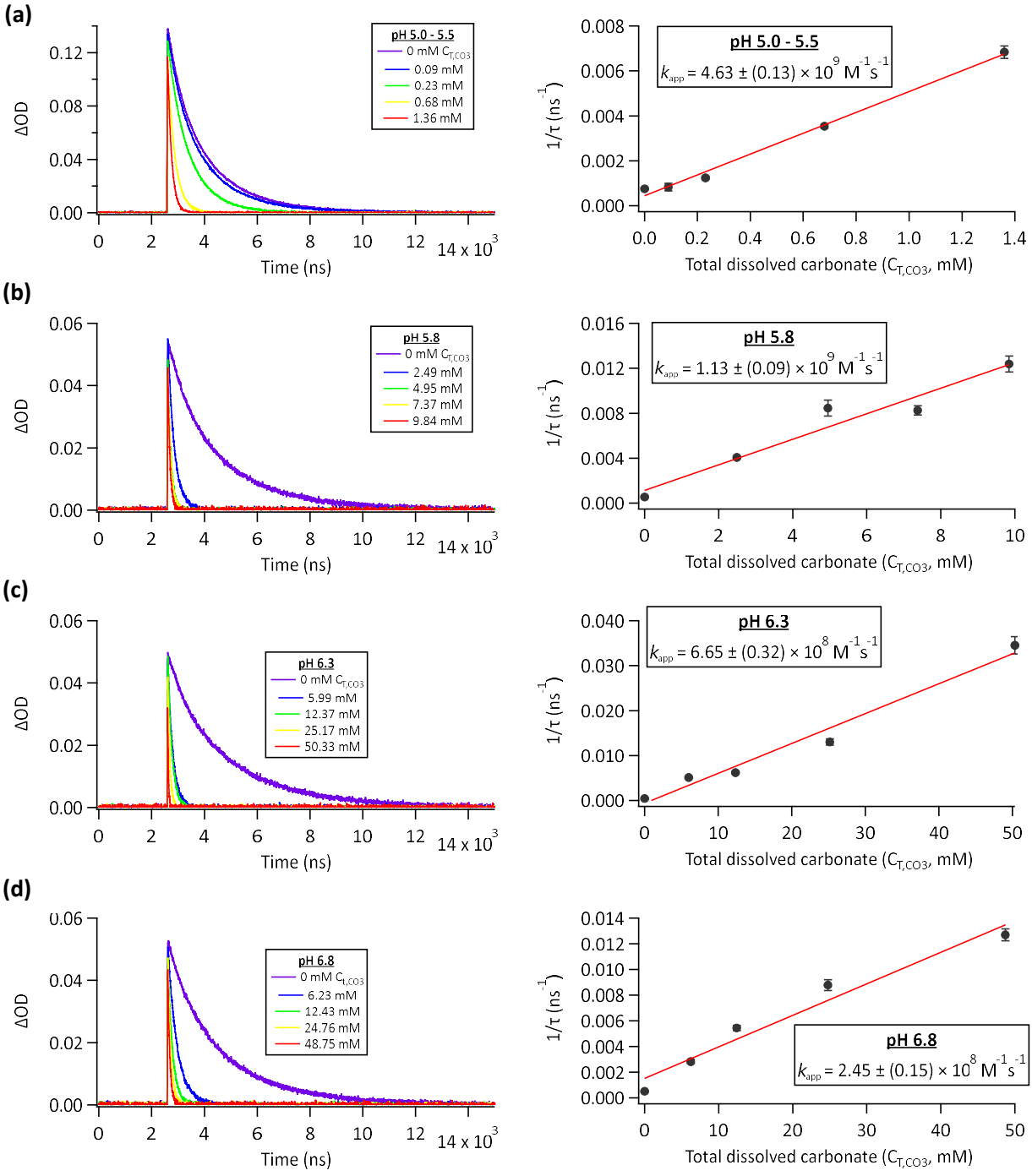

Figure S9. (Left) Transient absorbance traces depicting the decay of the characteristic 690 nm e^-_{aq} peak after photolyzing $K_4FE(CN)_6$ with 266 nm light. (Right) Corresponding Stern-Volmer plots. Error bars represent one standard deviation. Uncertainties of the k_{app} values represent standard errors of the regression-derived slope values using the *linest* function in Excel. Solution conditions are outlined in **Table 1**.

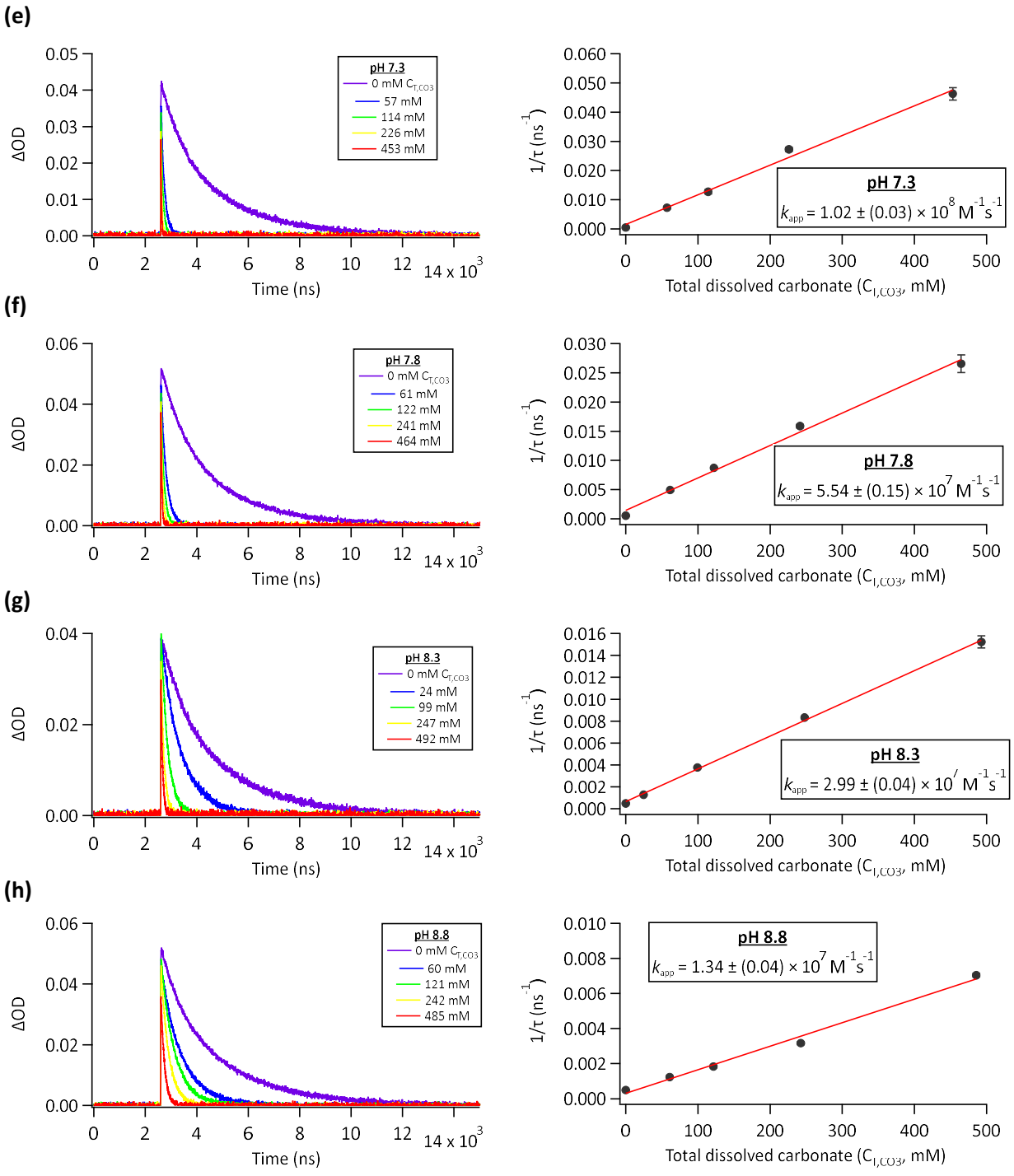

Figure S9. Continued.

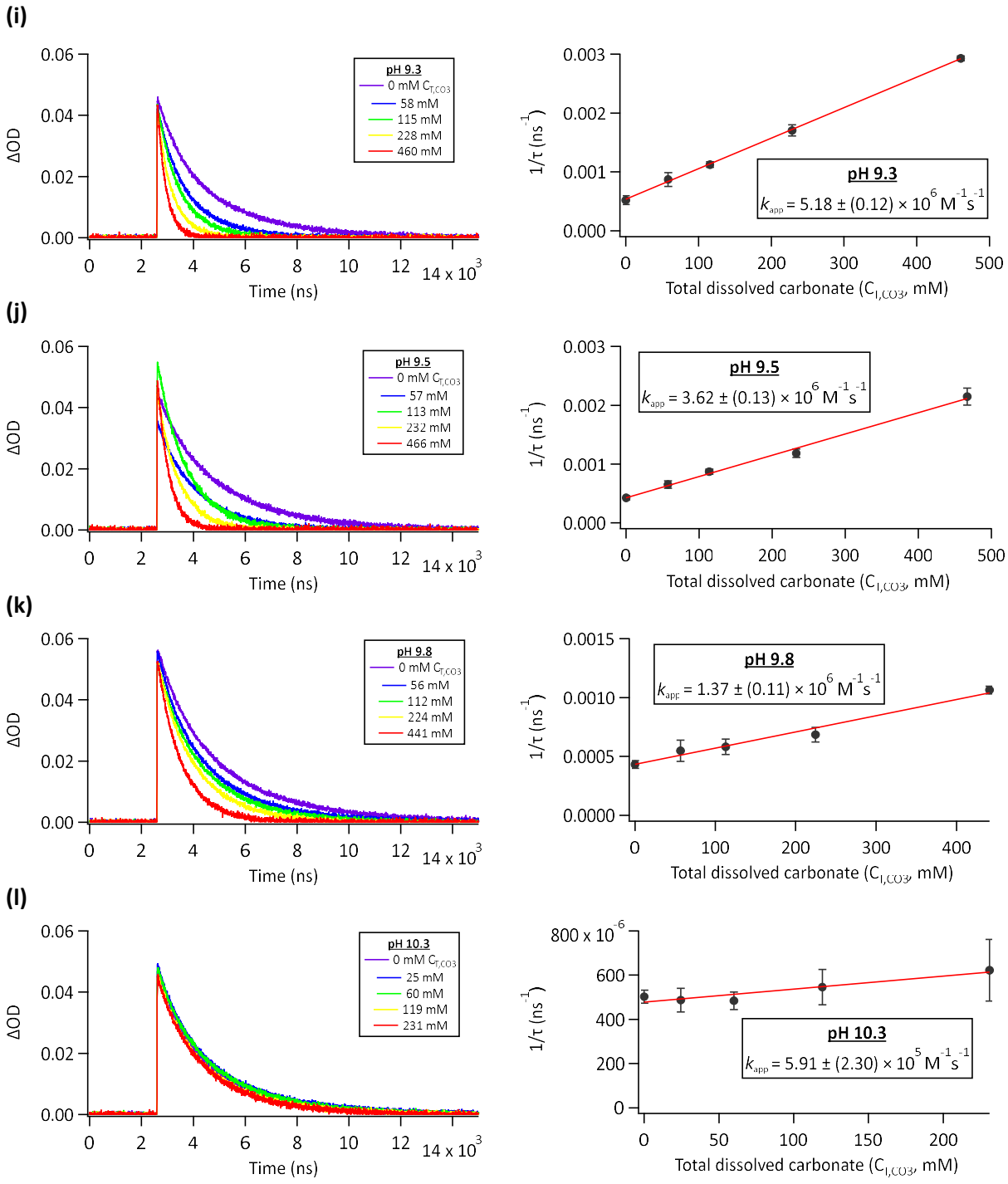

Figure S9. Continued.

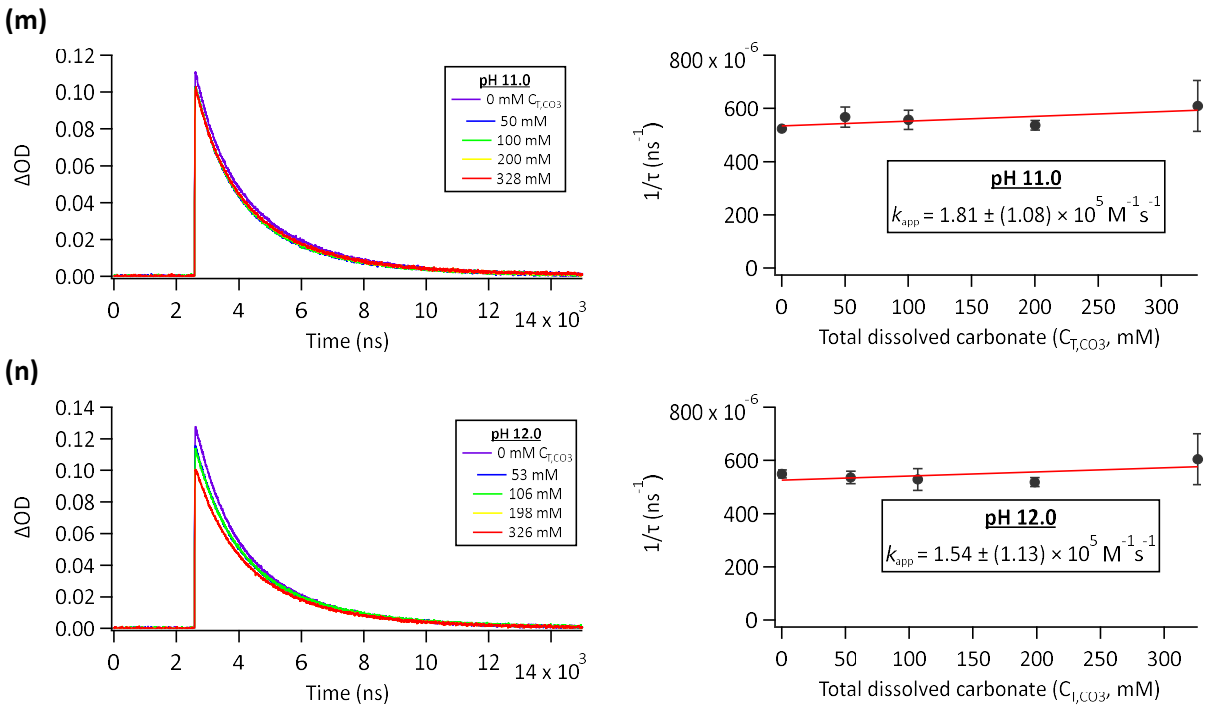

Figure S9. Continued.

References Cited in Supporting Information

(1) Thomas, J. K.; Gordon, S.; Hart, E. J. The Rates of Reaction of the Hydrated Electron in Aqueous Inorganic Solutions [1]. *J. Phys. Chem.* **1964**, *68* (6), 1524–1527. https://doi.org/10.1021/j100788a043.

(2) Li, X.; Zhang, P.; Jin, L.; Shao, T.; Li, Z.; Cao, J. Efficient Photocatalytic Decomposition of Perfluorooctanoic Acid by Indium Oxide and Its Mechanism. *Environmental Science & Technology* **2012**, *46* (10), 5528–5534. https://doi.org/10.1021/es204279u.

(3) Neta, P.; Huie, R. E.; Ross, A. B. Rate Constants for Reactions of Inorganic Radicals in Aqueous Solution. *Journal of Physical and Chemical Reference Data* **1988**, *17* (3), 1027–1284. https://doi.org/10.1063/1.555808.

(4) Sauer, M. C.; Crowell, R. A.; Shkrob, I. A. Electron Photodetachment from Aqueous Anions. 1. Quantum Yields for Generation of Hydrated Electron by 193 and 248 Nm Laser Photoexcitation of Miscellaneous Inorganic Anions. *The Journal of Physical Chemistry A* **2004**, *108* (25), 5490–5502. https://doi.org/10.1021/jp049722t.

(5) Shirom, M.; Stein, G. Excited State Chemistry of the Ferrocyanide Ion in Aqueous Solution. I. Formation of the Hydrated Electron. *The Journal of Chemical Physics* **1971**, *55* (7), 3372–3378. https://doi.org/10.1063/1.1676587.

(6) Hart, E. J.; Boag, J. W. **Absorption Spectrum of the Hydrated Electron in Water and in Aqueous Solutions**. *J. Am. Chem. Soc.* **1962**, *84* (21), 4090–4095. https://doi.org/10.1021/ja00880a025.

(7) Lisovskaya, A.; Bartels, D. M. Reduction of CO2 by Hydrated Electrons in High Temperature Water. *Radiation Physics and Chemistry* **2019**, *158*, 61–63. https://doi.org/10.1016/j.radphyschem.2019.01.017.

(8) Getoff, N. Possibilities on the Radiation-Induced Incorporation of CO2 and CO into Organic Compounds☆. *International Journal of Hydrogen Energy* **1994**, *19* (8), 667–672. https://doi.org/10.1016/0360-3199(94)90151-1.

(9) Jortner, J.; Ottolenghi, M.; Rabani, J.; Stein, G. Conversion of Solvated Electrons into Hydrogen Atoms in the Photo- and Radiation Chemistry of Aqueous Solutions. *The Journal of Chemical Physics* **1962**, *37* (10), 2488–2495. https://doi.org/10.1063/1.1733033.

(10) Dorfman, L. M.; Taub, I. A. **Pulse Radiolysis Studies. III. Elementary Reactions in Aqueous Ethanol Solution**. *J. Am. Chem. Soc.* **1963**, *85* (16), 2370–2374. https://doi.org/10.1021/ja00899a006.

(11) Phillips, G. O.; Power, D. M.; Sewart, M. C. G. Effects of γ-Irradiation on Sulphonamides. *Radiation Research* **1973**, *53* (2), 204. https://doi.org/10.2307/3573525.

(12) Maza, W. A.; Breslin, V. M.; Plymale, N. T.; DeSario, P. A.; Epshteyn, A.; Owrutsky, J. C.; Pate, B. B. Nanosecond Transient Absorption Studies of the PH-Dependent Hydrated Electron Quenching by HSO_3^-. *Photochem. Photobiol. Sci.* **2019**, *18* (6), 1526–1532. https://doi.org/10.1039/C9PP00063A.